7 Okusaka T, Okada S, Ueno H *et al.* Satellite lesions in patients with small hepatocellular carcinoma with reference to clinicopathologic features. *Cancer* 2002; **95**: 1931–7.
8 Kudo M. Local ablation therapy for hepatocellular carcinoma: current status and future perspectives. *J Gastroenterol* 2004; **39**: 205–14.
9 Nishijima N, Osaki Y, Kita R *et al.* Proposal of the radicality grading as a criterion for therapeutic effectiveness of RFA against hepatocellular carcinoma, in relation to the local recurrence rate. *Acta Hepatol Jpn* 2008; **49**: 192–99, (in Japanese).
10 Green S, Weiss GR. Southwest Oncology Group standard response criteria, endpoint definitions and toxicity criteria. *Invest New Drugs* 1992; **10**: 239–53.
11 Gehan EA, Tefft MC. Will there be resistance to the RECIST (Response Evaluation Criteria in Solid Tumors)? *J Natl Cancer Inst* 2000; **92**: 179–81.
12 Llovet JM, Beaugrand M. Hepatocellular carcinoma: present status and future prospects. *J Hepatol* 2003; **38** (Suppl 1): S136–49.4
13 Llovet JM, Di Bisceglie Am, Bruix J *et al.* Design and endpoints of clinical trials in hepatocellular carcinoma. *J Natl Cancer Inst* 2008; **100**: 698–711.
14 James K, Eisenhauer E, Christian M *et al.* Measuring response in solid tumors: unidimensional versus bidimensional measurement. *J Natl Cancer Inst* 1999; **91**: 523–8.
15 Park JO, Lee SI, Song SY *et al.* Measuring response in solid tumors: comparison of RECIST and WHO response criteria. *Jpn J Clin Oncol* 2003; **33**: 533–7.
16 The Liver Cancer Study Group of Japan. *The General Rules for the Clinical and Pathological Study of Primary Liver Cancer*, 2nd English edn, Tokyo: Kanehara, 1997.
17 The Liver Cancer Study Group of Japan. *The General Rules for the Clinical and Pathological Study of Primary Liver Cancer*. 5th Edn, Revised Version, Tokyo: Kanehara, 2009; (in Japanese).

APPENDIX I

TOVERALL EVALUATION OF treatment effects on liver cancer: a comparison between the World Health Organization (WHO) criteria, Response Evaluation Criteria in Solid Tumors (RECIST) and Response Evaluation Criteria in Cancer of the Liver (RECICL)

	WHO criteria (after 4 weeks)	RECIST (after 4 weeks)	RECICL (after 3 months)
Lesion evaluated	All evaluable lesions	All measurable lesions, target lesions (five lesions, a maximum of 10 lesions when lesions are present over 2 or more organs)	Target lesions (a maximum of five lesions when more than 5 lesions are present)
Evaluation method	Bi-dimensional measurement (changes in the product of the major axis and the diameter crossing the major axis at a right angle). Sum of the all lesions.	Uni-dimensional measurement (changes in the sum of the major axis)	Bi-dimensional measurement (changes in the product of the major axis and the diameter crossing the major axis at a right angle, non-stained regions on dynamic CT and/or lipiodol-deposited regions are measured as necrosis). Sum of the all target lesions.
Overall evaluation			
CR (complete response)	Disappearance of all lesions	Disappearance of all target lesions	100% tumor-necrotizing effect or 100% tumor size reduction rate
PR (partial response)	50% or greater disappearance of all lesions	30% or greater reduction of target lesions	A tumor-necrotizing effect or tumor size reduction rate between 50% and <100%
SD (stable disease)	Effects other than PR and PD	Effects other than PR and PD	Effects other than PR and PD
PD (progressive disease)	≥25% enlargement of a lesion or appearance of a new lesion	≥20% increase or appearance of a new lesion	≥25% enlargement of the tumor regardless of the necrotizing effect or appearance of a new lesion (categorized into three groups: intrahepatic solitary lesion, intrahepatic multiple lesions, and vascular invasion/extrahepatic spread).

APPENDIX II

Example RECICL Evaluation Sheet

Patient Age Male/female ID

1. **Description of Liver Cancer**
   (1) Past medical history
      (i) Method and date of definite diagnosis of liver cancer
      (ii) Past treatment history (only patients treat for recurrence)
   (2) Condition of liver cancer
      Tumor location, number and size of lesions, vascular invasion, macroscopic classification, macroscopic staging, histological type or degree of differentiation

2. **Description of Treatment Method**
   (1) Initial treatment or treatment for recurrence
   (2) Name of treatment (describe all treatments when multiple treatments were performed)
   (3) Details of treatment, including the reason for the discontinuation and the presence or absence of an adverse event when treatment is discontinued
   (4) Dates of initiation and completion of treatment

3. **Treatment Effect on Target Nodule (TE1, 2, 3, 4)**[*1] _____

   (Describe TE4a or 4b for local ablation)

   Assessment results: Lesion 1 _____
   Lesion 2 _____
   Lesion 3 _____
   Lesion 4 _____
   Lesion 5 _____

4. **Overall Evaluation (CR, PR, SD, PD)**[*2] _____

   Assessment results: _____

   When a new lesion appears in PD (new lesion: a, b, c)

Additional notes: tumor markers

Name of tumor marker	Before treatment	Lowest level within 3 months Time point ( )	6 months (only for radiotherapy)
AFP			
AFP-L3 fraction			
PIVKA-II (DCP)			

*1: Refer to Table 1. *2: Refer to Table 2.

World Journal of Radiology

Online Submissions: http://www.wjgnet.com/1949-8470office
wjr@wjgnet.com
doi:10.4329/wjr.v2.i7.249

World J Radiol 2010 July 28; 2(7): 249-256
ISSN 1949-8470 (online)

EDITORIAL

Hepatic malignancies: Correlation between sonographic findings and pathological features

Yasunori Minami, Masatoshi Kudo

Yasunori Minami, Masatoshi Kudo, Division of Gastroenterology and Hepatology, Department of Internal Medicine, Kinki University School of Medicine, 377-2, Ohno-Higashi, Osaka-Sayama 589-8511, Japan
Author contributions: Minami Y wrote the manuscript; Kudo M revised the article for important intellectual content.
Correspondence to: Masatoshi Kudo, MD, PhD, Division of Gastroenterology and Hepatology, Department of Internal Medicine, Kinki University School of Medicine, 377-2, Ohno-Higashi, Osaka-Sayama 589-8511, Japan. m-kudo@med.kindai.ac.jp
Telephone: +81-72-3660221 Fax: +81-72-3672880
Received: March 30, 2010 Revised: May 27, 2010
Accepted: June 3, 2010
Published online: July 28, 2010

Abstract

Ultrasonography (US) findings are inevitably based on pathological features. Knowledge of the pathological features of hepatic malignancies such as hepatocellular carcinoma (HCC), liver metastasis and intrahepatic cholangiocarcinoma is essential for correct US diagnosis and appropriate management. One type of hepatocarcinogenesis is step-wise development from a low-grade dysplastic nodule (DN), high-grade DN, high-grade DN with malignant foci, and well-differentiated HCC, to classical HCC. The intranodular blood supply changes in accordance with this progression. Moreover, the malignant potential tends to change as the macroscopic configuration progresses. Therefore, typical US findings of advanced HCC are a mosaic pattern, septum formation, peripheral sonolucency (halo), lateral shadow produced by fibrotic pseudocapsule, posterior echo enhancement, arterial hypervascularity with dilated intratumoral blood sinusoids, and perinodular daughter nodule formation. Bull's eye appearance is a common presentation of metastases from gastrointestinal (GI) adenocarcinomas, and represents histological findings that show an area of central necrosis surrounded by a zonal area of viable tumor. Thick zonal area reflects the layer of viable cells that are fed by minute tumor vessels. US imaging features of liver metastases from the GI tract are as follows: Bull's eye appearance, multiple masses, irregular tumor border, arterial rim-like enhancement, and hypoenhancement in the late vascular phase. Most intrahepatic cholangiocarcinomas are ductal adenocarcinomas. The bile ducts peripheral to the tumor are usually dilated because of obstruction by tumors. US imaging features of mass-forming cholangiocarcinoma are as follows: peripheral bile duct dilatation, irregular tumor border, arterial enhancement due to minute intratumoral blood sinusoids, and hypoenhancement in the late vascular phase.

Key words: Hepatocellular carcinoma; Liver metastasis; Intrahepatic cholangiocarcinoma; Sonography; Pathology

Peer reviewer: Hui-Xiong Xu, MD, PhD, Professor, Department of Medical Ultrasonics, Institute of Diagnostic and Interventional Ultrasound, Sun Yat-Sen University, 58 Zhongshan Road 2, Guangzhou 510080, Guangdong Province, China

Minami Y, Kudo M. Hepatic malignancies: Correlation between sonographic findings and pathological features. *World J Radiol* 2010; 2(7): 249-256 Available from: URL: http://www.wjgnet.com/1949-8470/full/v2/i7/249.htm DOI: http://dx.doi.org/10.4329/wjr.v2.i7.249

INTRODUCTION

Recent advances in digital technologies have resulted in remarkable developments in the field of imaging modalities[1]. Ultrasonography (US) is one of the diagnostic tools that have shown significant improvement within the last decade[2-7]. For the diagnosis of liver tumors, US examination has the advantages of real-time observation, simple technique and non-invasiveness[8-13]. This modality is being used worldwide with high frequency as a reli-

able method for the initial diagnosis of liver tumors[14-19]. Color Doppler and power Doppler have increased the sensitivity for hepatic lesion detection compared to that of gray-scale US[20-25]. Furthermore, the application of microbubble contrast agents provides details of the hemodynamics, which are useful for the detection and characterization of liver tumors[26-31].

Even if advances in imaging technology increase further, US findings are inevitably based on the pathological features. Therefore, knowledge of disease conditions and pathological features is essential to comprehend the findings on US images.

This paper reviews the diagnosis of hepatic malignancies contrasted between US images and pathological features.

HEPATOCELLULAR CARCINOMA

Disease conditions and pathological features

Hepatocellular nodules associated with liver cirrhosis are divided into six categories according to the classification proposed by the International Working Party of World Congress of Gastroenterology in 1994: namely, large regenerative nodule, low-grade dysplastic nodule (DN), high-grade DN, high-grade DN with malignant foci, well-differentiated hepatocellular carcinoma (HCC), and HCC with Edmondson II or higher, which is called classical HCC[32-36]. Among these nodules, two models of hepatocarcinogenesis are now hypothesized. One is *de novo* carcinogenesis, and the other is stepwise development from low-grade DN, high-grade DN, high-grade DN with malignant foci, and well-differentiated HCC, to classical HCC. The intranodular blood supply changes with the progression of human hepatocarcinogenesis from DN to overt HCC[32-36] (Figure 1). The portal tracts, including the portal vein and hepatic artery, decrease with the increasing grade of malignancy and are virtually absent in nodules. In contrast, abnormal arteries due to tumor angiogenesis develop in atypical adenomatous hyperplasia (high-grade DN) during the course of hepatocarcinogenesis, and are markedly increased in number in moderately differentiated HCCs. The intranodular vasculature changes in a stepwise manner as the grade of malignancy increases[32-36]. In the course of hepatocarcinogenesis, arterial and portal supply decreases (due to a decrease in the portal tracts), and arterial supply returns to a level equivalent (due to newly formed abnormal arteries) to the surrounding liver, while portal supply continues to decrease, and finally portal supply vanishes and only arterial blood (from newly formed abnormal arteries) supplies the lesion (classical HCC). Therefore, high-grade DN is usually hypodense relative to the surrounding liver. However, early-stage well-differentiated HCC often shows isodensity because the increased abnormal arterial supply compensates for the decreased normal hepatic arterial supply[34-36].

Macroscopic configurations of HCC

In the classification proposed by the Liver Cancer Study Group of Japan, macroscopic configurations of HCC are divided into five types, namely the small nodular type with indistinct margins, simple nodular type, simple nodular type with extranodular growth, confluent multinodular type, and infiltrative type[37,38] (Figure 2). The malignant potentials tend to change in accordance with the progression of macroscopic configurations[38].

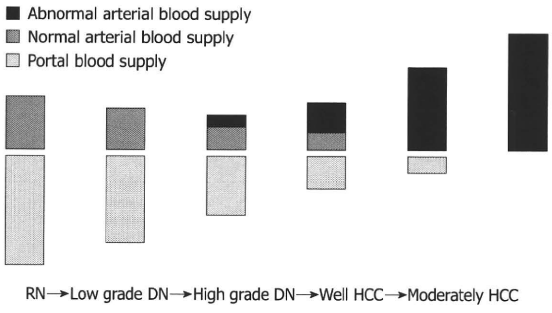

Figure 1 Changes in intranodular blood supply with the progression of hepatocarcinogenesis from dysplastic nodule to hepatocellular carcinoma. RN: Regenerative nodule; DN: Dysplastic nodule; HCC: Hepatocellular carcinoma.

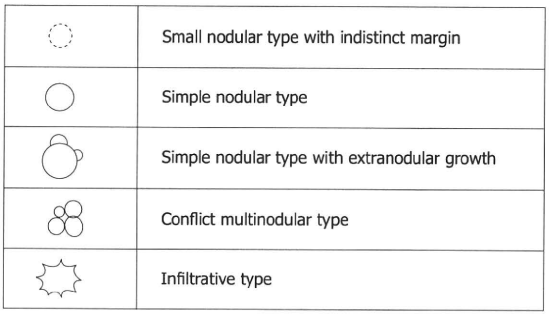

Figure 2 Macroscopic configurations of hepatocellular carcinoma.

In the small nodular type with indistinct margins, approximately 85% of nodules consist of well-differentiated cancerous tissue with a replacing growth at the boundary, and many portal tracts are retained in the tumor with immature fibrous capsule formation. When such tumors reach 1.5-2.0 cm in diameter, moderately or poorly differentiated cancer tissues develop within the well-differentiated cancer tissue. When less differentiated cancerous tissues within the well-differentiated cancer nodules proliferate in an expansive fashion, a "nodule-in-nodule" appearance is frequently seen.

The simple nodular type exhibits a round or nearly round shape, and demonstrates a clear boundary with non-cancerous tissue, and it often has an obvious capsule. Some tumors appear intersected by thin fibrous septa, but these tumors are round, and have the appearance of a single expanding nodule. Moderately differentiated cancerous tissue accounts for approximately 75% of the simple nodular type of HCC, and approximately 20% show portal invasion on histology.

In the simple nodular type with extranodular growth,

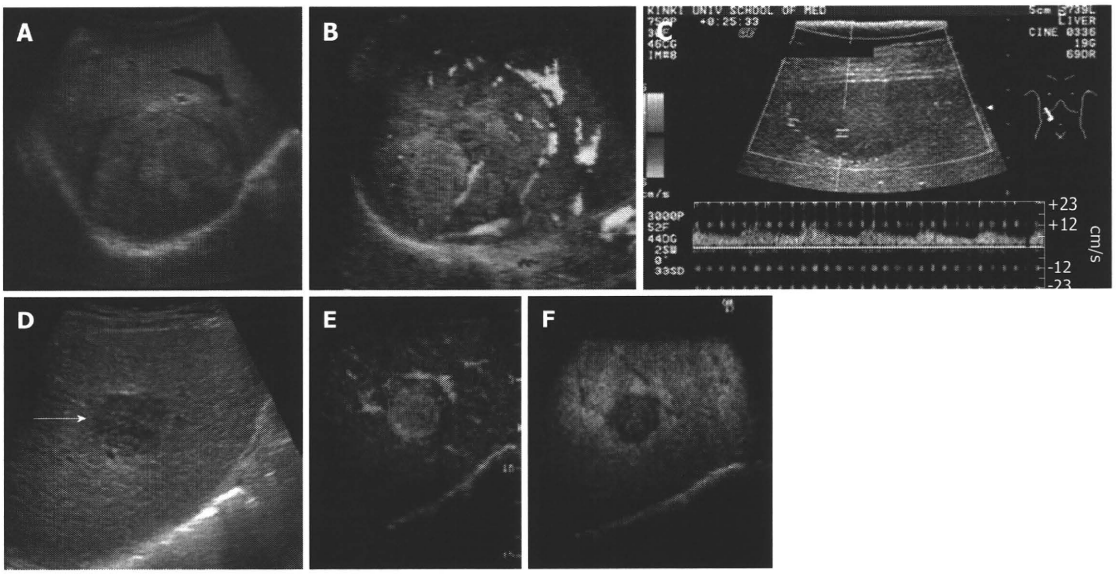

Figure 3 Advanced hepatocellular carcinoma. A: The nodule had a halo image and mosaic pattern in segment 8 of the liver on B-mode ultrasonography; B: Power Doppler imaging showed hypervascularity of the tumor; C: Color Doppler imaging showed intratumoral blood flow. Arterial pulsatile waveforms could be detected by pulsed Doppler images; D: The image of a simple nodular type with extranodular growth (arrow) was obtained on B-mode ultrasonography (US); E: Contrast harmonic US showed enhancement of hepatocellular carcinoma in early vascular phase after administration of perfluorocarbon microbubbles; F: Contrast harmonic US depicted the defect image in the post-vascular phase.

well-differentiated histological characteristics are present in only 12.5% of cases. The simple nodular type of HCC with extranodular growth is well developed in contrast to the delicate fibrous septa that are occasionally present in the small nodular type with indistinct margins. Most of the simple nodular type with extranodular growth demonstrates moderately differentiated HCC.

Confluent multinodular type tumor is formed by several small contiguous tumor nodules. In confluent multinodular type tumors, the margin of the whole tumor appears rugged because of the projection of each nodule. In addition, the internodular fibrous tissue of confluent multinodular type tumors is well developed. This unique appearance probably reflects the extension of tumor by growth replacement from one pseudolobule into its neighbors. Most of the confluent multinodular type is classified as moderately to poorly differentiated HCC.

The infiltrative type of tumor is classified as the poorly demarcated nodular type. The most important reason for classifying this tumor separately is that grossly the entire border is obscure. Histologically, the entire boundary between cancerous and non-cancerous parenchyma is composed of small nests of cancer cells that infiltrate the interlobular septa, similar to the infiltrative pattern of adenocarcinoma. Most infiltrative type tumor is diagnosed in poorly differentiated HCC or mixed HCC/cholangiocarcinoma.

US imaging of advanced HCC

Typical US findings of advanced HCC are a mosaic pattern, septum formation, peripheral sonolucency (halo), lateral shadow produced by fibrotic pseudocapsule, posterior echo enhancement, arterial hypervascularity with dilated intratumoral blood sinusoids, and perinodular daughter nodule formation (Figure 3).

Internal mosaic architecture and capsule formation are major macroscopic features of typical moderately differential HCCs[39-41]. The halo sign and lateral shadows correspond to the thin fibrous capsule of the HCC. Correspondence between sonographic halo sign and histological capsule has been reported as 90.1%, and that between the presence of extracapsular invasion on US and that on histology as 88.0%. The presence of extracapsular invasion on US is a predisposing factor for the development of tumor recurrence.

Posterior echo enhancement is due to the softness of the HCC[42]. However, posterior echo enhancement is not specific for HCC, as this finding is also observed with similarly frequency in hemangiomas.

The spread of HCC along the portal vein results in daughter nodule formation. In HCC, the hepatic artery is the feeding vessel and the portal vein serves mainly as an efferent vessel. Tumor cells invade efferent vessels by budding, extension to the vascular cavity, and then extending beyond the capsule to the portal vein branches. In more advanced cases of HCC, portal tumor thrombi, biliary invasion, and hepatic vein invasion are also observed, which strongly indicates a diagnosis of HCC.

A basket pattern on color Doppler images and/or power Doppler images has been described; this pattern represents a fine network of arterial vessels that surrounds the tumor nodules[43,44]. Typical color Doppler findings in advanced HCC are afferent pulsatile waveform signals, intratumoral pulsatile waveform signals associated with intratumoral

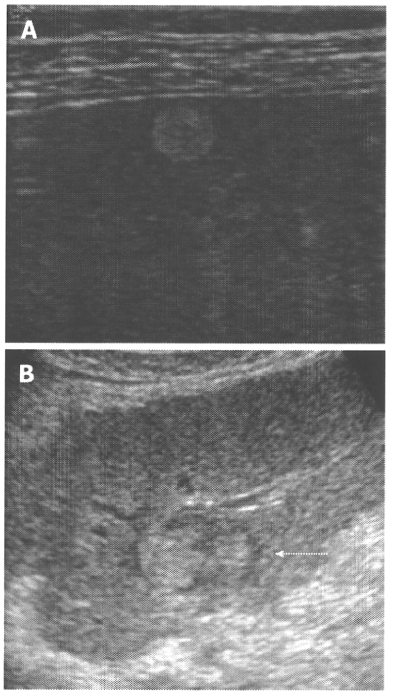

Figure 4 Early hepatocellular carcinoma. A: A nodule that was 1.5 cm in diameter in segment 5 of the liver was shown as highly echoic because of fatty changes in the nodule; B: A nodule-in-nodule appearance (arrow) was demonstrated as a hyperechoic tumor within a hypoechoic nodule.

continuous waveform signals, and efferent continuous waveform signals. Of the several parameters that can be obtained with Doppler spectral analysis, maximum flow velocity and pulsatility index (PI) are very important in the differential diagnosis of hepatic tumors. The PI in HCC is much higher than that in hemangioma.

Hepatic carcinogenesis is described as a multi-step process in which progressive arterialization and gradual loss of portal vessels are the principal features[45,46]. It is evident that vascular enhancement is related to the evolution of the lesion. Thus, during the arterial phase, DNs or early HCC usually appear hypo or isovascularized, while advanced HCCs are hypervascularized. Contrast-enhanced US can show selective enhancement in the arterial phase, which differentiates HCCs from regenerative nodules and DNs[4-6].

US imaging of early HCC

The imaging features of early HCC (highly well-differentiated HCC) are as follows: bright loop appearance, arterial hypovascularity and internal portal tracts or portal blood supply. Hypervascular foci in the nodule occasionally demonstrate a nodule-in-nodule appearance (Figure 4).

Bright loop appearance is defined as hypoechoic nodules in a hyperechoic tumor[47]. A nodule-in-nodule appearance might also appear as a hyperechoic tumor within a hypoechoic nodule[25,46]. Hyperechoic HCC nodules represent well-differentiated HCC with fatty changes, whereas an inner hypoechoic lesion represents moderately differentiated HCC without fatty changes. On US screening for HCC, these appearances are often observed in HCC nodules that measure 11-20 mm in diameter. Histological examination has demonstrated that bright loop appearance and nodule-in-nodule appearance of HCC on US are associated with tumor progression and dedifferentiation to moderately differentiated HCC within well-differentiated HCC with fatty changes.

Typical findings of early HCC are afferent continuous waveform signals, which reflect a feeding portal flow, which is rarely associated with pulsatile wave-form signals[48]. Thus, with afferent blood flow on Doppler US imaging, constant waveform signals that reflect portal inflow are a characteristic finding in DNs and early well-differentiated HCC.

Half of the well-differentiated HCCs wash out slowly during the late phase on contrast-enhanced US and the average washout time was significantly different from that of moderately to poorly differentiated HCCs[17,21,23,46]. Microbubbles continuously infusing the tumor through the portal vein could be the pathological basis of slow washout. Furthermore, well-differentiated HCCs consist of a trabecular pattern of cell cords and abundant sinusoids that may cause stagnation and slow clearance of microbubbles. Conversely, less differentiated HCCs contain fewer sinusoids and are mainly fed by the hepatic artery, which could cause the difference in washout time compared with that of well-differentiated HCCs.

LIVER METASTASIS

Disease conditions and pathological features

The liver is the organ second most commonly affected by metastatic disease. The most common primary sites are the gastrointestinal (GI) tract, lung, breast and head and neck[49-52]. Therefore, liver metastases vary in size, shape, vascularity, and growth pattern. However, most liver metastases are multiple and show the so-called "cluster sign". In 77% of patients with liver metastases, both lobes are involved, whereas metastasis is solitary in only 10% of cases[53]. Most metastatic tumors of the liver are expansive or infiltrative. Although most metastases are generally hypovascular, metastases often show the same degree of vascularity as the primary tumor[54]. Calcification can be seen in metastases from colon, stomach, breast, and other organs. Fundamentally, liver metastases occur in patients without liver cirrhosis[54].

In metastases from the GI tract, intratumoral fibrous septum and capsule formation are macroscopically rare. Hypervascular metastases are uncommon, however, arterial vascularity of metastases develops finely near the border. Large metastases often outgrow their blood supply and subsegment hypoxia causes a necrotic region at the center of the tumor[54].

In addition, metastatic carcinoma from the breast or pancreas induces an intense fibrous or sclerosing reaction around the tumor, which leads to fibrous scar formation[55]. In 7%-15% of patients, tumor thrombi occlude

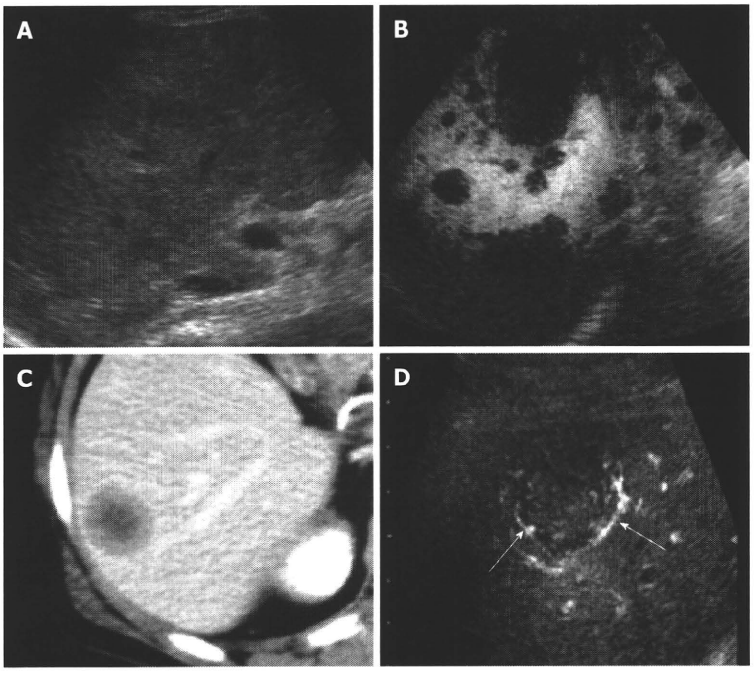

Figure 5 Liver metastasis. A: Multiple masses were seen in the liver by B-mode ultrasonography (US); B: Multiple defects were seen by Sonazoid-enhanced US in the post-vascular phase; C: Portal phase dynamic scan detected a hypoenhanced nodule in segment 6 of the liver; D: Peripheral enhancement of the nodule (arrows) was obtained by Sonazoid-enhanced ultrasonography in the early vascular phase.

the portal vein, the hepatic vein, or both. In the presence of mucin secretion, necrosis, and phosphate activity, metastases can develop calcification that is detectable radiographically.

US imaging

US imaging features of liver metastases from the GI tract are as follows: Bull's eye appearance, multiple masses, absence of liver cirrhosis, irregular tumor border, arterial rim-like enhancement, and hypoenhancement in the late vascular phase (Figure 5).

Bull's eye or target lesion is a common presentation of metastases from the GI tract[56]. Sonography also shows multiple round and/or hypoechoic masses with irregular borders[57]. A Bull's eye appearance represents histological findings of an area that shows central coagulative necrosis surrounded by a zonal area of viable tumor. The surrounding zonal area appears thick, and reflects a layer of viable cells. Calcified metastases might demonstrate shadows when they are densely echogenic. Then, colon cancer is the most likely cause in a patient with unknown primary tumor when calcified liver metastases are demonstrated by US.

Color or power Doppler US can show intratumoral vascularity in the peripheral hypoechoic zone, in which viable tumor cells are proliferating[58]. Actually, these signals appear to be poor because the density of tumor vasculature is lower than that of moderately differentiated HCC. However, in patients with metastasis from renal cell carcinoma or sarcoma, intratumoral flow can be demonstrated because of its hypervascularity.

Contrast-enhanced US of the liver with SonoVue provides a significantly higher sensitivity in the detection of liver metastases compared to that of unenhanced sonography, and identifies up to 40% more metastases[59-61]. It has been reported that the presence of rim-like enhancement with peripheral tumor vessels (sensitivity, 88.1%; specificity, 100%) is the typical pattern[62]. Contrast-enhanced US in the late phase provides a marked improvement in the detection of hepatic metastases as areas of hypoenhancement, and can be advantageous in detecting small metastases compared with computed tomography and magnetic resonance imaging[63-65].

INTRAHEPATIC CHOLANGIOCARCINOMA

Disease conditions and pathological features

Intrahepatic cholangiocarcinoma is a slow-growing ductal adenocarcinoma in the liver; it is relatively rare and comprises 3%-7% of malignant liver tumors[66-69]. The bile ducts are dilated because of obstruction by tumors[70,71]. Intrahepatic cholangiocarcinoma, unlike HCC, is not usually related to liver cirrhosis. However, hepatitis C virus infection has also been reported to be a risk factor for cholangiocarcinoma[72]. The Liver Cancer Study Group of Japan has proposed a classification of intrahepatic cholangiocarcinoma based on macroscopic features: mass-forming, periductal infiltrating, and intraductal, or mixed mass-forming, and periductal infiltrating[73,74]. More than half of intrahepatic cholangiocarcinomas are classified as the mass-forming type.

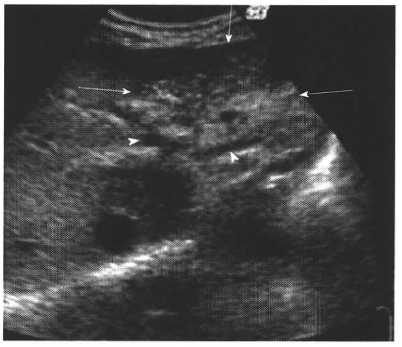

Figure 6 Intrahepatic cholangiocarcinoma (mass-forming type). B-mode ultrasonography showed mixed echogenicity with irregular borders (arrows) in the left lateral lobe. The intrahepatic bile duct peripheral to the tumor was dilated (arrowheads).

A mass-forming intrahepatic cholangiocarcinoma is usually large. On gross specimens, the tumor is firm and whitish gray because of its large amount of fibrous stroma[75]. The margin is well circumscribed and wavy or lobulated. Central necrosis might be present. Multicentricity, especially around the main tumor, is common, probably because of the propensity of the tumor to invade the adjacent peripheral branches of the portal vein[75-77]. It easily spreads to the lymph nodes. Most of the mass-forming intrahepatic cholangiocarcinomas are poorly or moderately differentiated[75].

US imaging

US imaging features of mass-forming cholangiocarcinoma are as follows: peripheral bile duct dilatation, absence of liver cirrhosis, irregular tumor border, arterial enhancement due to minute intratumoral blood sinusoids, and hypoenhancement in the late vascular phase (Figure 6).

The bile ducts peripheral to the tumor are usually dilated because of obstruction by the tumor, however, the US findings of intrahepatic cholangiocarcinoma are fundamentally very similar to those described in liver metastases[71]. Mass-forming cholangiocarcinomas can be hypoechoic, hyperechoic, or have mixed echogenicity, with irregular borders. Peripheral cholangiocarcinoma can appear as a solitary mass or as diffusely abnormal liver echotexture. Because of their nonspecific symptomatology, mass-forming lesions are generally far advanced when detected by US. In addition, mass-forming lesions might mimic HCC or metastases on B-mode US[70].

Color Doppler US typically shows a poor color signal in cholangiocarcinoma compared with HCC, which is hypervascular. Hence, color Doppler US is helpful in differentiating vessels from dilated ducts and can provide information regarding the status of vessels. It is considered highly accurate in detecting neoplastic involvement of the portal vein. In the study by Neumaier *et al*[78], the sensitivity of color Doppler US for portal vein occlusion was 100% and that for portal vein infiltration was 83%, with 100% specificity. However, there was poor sensitivity in detecting infiltration of the hepatic artery (43%) and metastases to regional lymph nodes (37%), liver (66%), and peritoneum (33%)[78].

Although the imaging findings of peripheral cholangiocarcinoma showed certain characteristics on low-mechanical index (MI) contrast-enhanced sonography, contrast-enhanced US findings are fundamentally similar to those described for liver metastases. It has been reported[79] that all peripheral cholangiocarcinomas show inhomogeneous enhancement during the arterial phase, such as irregular, peripheral, rim-like hyperenhancement (44.4%), inhomogeneous hyperenhancement (11.1%), or inhomogeneous hypoenhancement (44.4%). However, all cholangiocarcinomas show hypoenhancement in the late vascular phase.

CONCLUSION

Worldwide, US imaging plays an important role not only in screening, evaluating, staging and monitoring disease, but also in surveillance following tumor ablation. Advances in imaging techniques have increased our ability to detect and characterize focal liver lesions. The gross appearances of hepatic malignancies correlate with the pathological and US imaging findings, therefore, the macroscopic types can be a significant independent prognostic factor. Knowledge of the pathological features of liver tumors is essential for correct US diagnosis and appropriate management. Some pathological images can enhance our understanding of liver tumors.

REFERENCES

1 **Maruyama K**, Yoshikawa M, Yokosuka O. Contrast-enhanced ultrasonography: a recent application for the diagnosis and treatment of hepatocellular carcinoma. *JNMA J Nepal Med Assoc* 2008; **47**: 156-166

2 **Kudo M**. Imaging diagnosis of hepatocellular carcinoma and premalignant/borderline lesions. *Semin Liver Dis* 1999; **19**: 297-309

3 **Kudo M**. Contrast harmonic ultrasound is a breakthrough technology in the diagnosis and treatment of hepatocellular carcinoma. *J Med Ultrason* 2001; **28**: 79-81

4 **Ding H**, Kudo M, Onda H, Suetomi Y, Minami Y, Maekawa K. Hepatocellular carcinoma: depiction of tumor parenchymal flow with intermittent harmonic power Doppler US during the early arterial phase in dual-display mode. *Radiology* 2001; **220**: 349-356

5 **Ding H**, Kudo M, Maekawa K, Suetomi Y, Minami Y, Onda H. Detection of tumor parenchymal blood flow in hepatic tumors: value of second harmonic imaging with a galactose-based contrast agent. *Hepatol Res* 2001; **21**: 242-251

6 **Ding H**, Kudo M, Onda H, Suetomi Y, Minami Y, Chung H, Kawasaki T, Maekawa K. Evaluation of posttreatment response of hepatocellular carcinoma with contrast-enhanced coded phase-inversion harmonic US: comparison with dynamic CT. *Radiology* 2001; **221**: 721-730

7 **Minami Y**, Kudo M, Kawasaki T, Kitano M, Chung H, Maekawa K, Shiozaki H. Transcatheter arterial chemoembolization of hepatocellular carcinoma: usefulness of coded phase-inversion harmonic sonography. *AJR Am J Roentgenol* 2003; **180**: 703-708

8 **Wen YL**, Kudo M, Zheng RQ, Minami Y, Chung H, Suetomi Y, Onda H, Kitano M, Kawasaki T, Maekawa K. Radiofrequency ablation of hepatocellular carcinoma: therapeutic response using contrast-enhanced coded phase-inversion harmonic sonography. *AJR Am J Roentgenol* 2003; **181**: 57-63

9 **Wen YL**, Kudo M, Maekawa K, Minami Y, Chung H, Suetomi Y, Onda H, Kitano M, Kawasaki T. Contrast advanced dynamic flow imaging and contrast pulse subtraction imaging: Preliminary results in hepatic tumors. *J Med Ultrason* 2002; **29**: 195-204

10 **Wen YL**, Kudo M, Minami Y, Chung H, Suetomi Y, Onda H, Kitano M, Kawasaki T, Maekawa K. Contrast-enhanced agent detection imaging: Early experience in hepatocellular carcinoma. *J Med Ultrason* 2003; **30**: 77-84

11 **Wen YL**, Kudo M, Minami Y, Chung H, Suetomi Y, Onda H, Kitano M, Kawasaki T, Maekawa K. Value of new contrast harmonic technique for detecting tumor vascularity in hepatocellular carcinoma: Preliminary results. *J Med Ultrason* 2003; **30**: 85-92

12 **Wen YL**, Kudo M, Minami Y, Chung H, Suetomi Y, Onda H, Kitano M, Kawasaki T, Maekawa K. Detection of tumor vascularity in hepatocellular carcinoma with contrast-enhanced Dynamic Flow imaging: Comparison with contrast-enhanced power Doppler imaging. *J Med Ultrason* 2003; **30**: 141-151

13 **Wang WP**, Ding H, Qi Q, Mao F, Xu ZZ, Kudo M. Characterization of focal hepatic lesions with contrast-enhanced C-cube gray scale ultrasonography. *World J Gastroenterol* 2003; **9**: 1667-1674

14 **Wen YL**, Kudo M, Zheng RQ, Ding H, Zhou P, Minami Y, Chung H, Kitano M, Kawasaki T, Maekawa K. Characterization of hepatic tumors: value of contrast-enhanced coded phase-inversion harmonic angio. *AJR Am J Roentgenol* 2004; **182**: 1019-1026

15 **Wen YL**, Zhou P, Kudo M. Detection of intratumoral vascularity in small hepatocellular carcinoma by coded phase inversion harmonics. *Intervirology* 2004; **47**: 169-178

16 **Zheng RQ**, Zhou P, Kudo M. Hepatocellular carcinoma with nodule-in-nodule appearance: demonstration by contrast-enhanced coded phase inversion harmonic imaging. *Intervirology* 2004; **47**: 184-190

17 **Kudo M**. Early detection and curative treatment of early-stage hepatocellular carcinoma. *Clin Gastroenterol Hepatol* 2005; **3**: S144-S148

18 **Zheng RQ**, Kudo M. Hepatic angiomyolipoma: identification of an efferent vessel to be hepatic vein by contrast-enhanced harmonic ultrasound. *Br J Radiol* 2005; **78**: 956-960

19 **Zheng RQ**, Zhang B, Kudo M, Sakaguchi Y. Hemodynamic and morphologic changes of peripheral hepatic vasculature in cirrhotic liver disease: a preliminary study using contrast-enhanced coded phase inversion harmonic ultrasonography. *World J Gastroenterol* 2005; **11**: 6348-6353

20 **Inoue T**, Kitano M, Kudo M, Sakamoto H, Kawasaki T, Yasuda C, Maekawa K. Diagnosis of gallbladder diseases by contrast-enhanced phase-inversion harmonic ultrasonography. *Ultrasound Med Biol* 2007; **33**: 353-361

21 **Kudo M**. New sonographic techniques for the diagnosis and treatment of hepatocellular carcinoma. *Hepatol Res* 2007; **37** Suppl 2: S193-S199

22 **Zhou P**, Kudo M, Minami Y, Chung H, Inoue T, Fukunaga T, Maekawa K. What is the best time to evaluate treatment response after radiofrequency ablation of hepatocellular carcinoma using contrast-enhanced sonography? *Oncology* 2007; **72** Suppl 1: 92-97

23 **Kudo M**, Hatanaka K, Maekawa K. Sonazoid-enhanced ultrasound in the diagnosis and treatment of hepatic tumors. *J Med Ultrasound* 2008; **16**: 130-139

24 **Kudo M**, Hatanaka K, Maekawa K. Defect reperfusion imaging, a newly developed novel technology using Sonazoid in the treatment of hepatocellular carcinoma. *J Med Ultrasound* 2008; **16**: 169-176

25 **Inoue T**, Kudo M, Hatanaka K, Takahashi S, Kitai S, Ueda T, Ishikawa E, Hagiwara S, Minami Y, Chung H, Ueshima K, Maekawa K. Imaging of hepatocellular carcinoma: qualitative and quantitative analysis of postvascular phase contrast-enhanced ultrasonography with sonazoid. Comparison with superparamagnetic iron oxide magnetic resonance images. *Oncology* 2008; **75** Suppl 1: 48-54

26 **Xia Y**, Kudo M, Minami Y, Hatanaka K, Ueshima K, Chung H, Hagiwara S, Inoue T, Ishikawa E, Kitai S, Takahashi S, Tatsumi C, Ueda T, Hayaishi S, Maekawa K. Response evaluation of transcatheter arterial chemoembolization in hepatocellular carcinomas: the usefulness of sonazoid-enhanced harmonic sonography. *Oncology* 2008; **75** Suppl 1: 99-105

27 **Kudo M**, Minami Y. Radiofrequency ablation therapy under harmonic imaging guidance for the recurring cancer after local therapy for HCC: a randomized controlled study with RFA under B-mode guidance. *Ultrasound Med Biol* 2003; **29**: S145

28 **Minami Y**, Kudo M, Kawasaki T, Chung H, Ogawa C, Shiozaki H. Treatment of hepatocellular carcinoma with percutaneous radiofrequency ablation: usefulness of contrast harmonic sonography for lesions poorly defined with B-mode sonography. *AJR Am J Roentgenol* 2004; **183**: 153-156

29 **Minami Y**, Kudo M, Chung H, Kawasaki T, Yagyu Y, Shimono T, Shiozaki H. Contrast harmonic sonography-guided radiofrequency ablation therapy versus B-mode sonography in hepatocellular carcinoma: prospective randomized controlled trial. *AJR Am J Roentgenol* 2007; **188**: 489-494

30 **Minami Y**, Kudo M, Kawasaki T, Chung H, Ogawa C, Shiozaki H. Percutaneous radiofrequency ablation guided by contrast-enhanced harmonic sonography with artificial pleural effusion for hepatocellular carcinoma in the hepatic dome. *AJR Am J Roentgenol* 2004; **182**: 1224-1226

31 **Kono Y**, Lucidarme O, Choi SH, Rose SC, Hassanein TI, Alpert E, Mattrey RF. Contrast-enhanced ultrasound as a predictor of treatment efficacy within 2 weeks after transarterial chemoembolization of hepatocellular carcinoma. *J Vasc Interv Radiol* 2007; **18**: 57-65

32 **Kanai T**, Hirohashi S, Upton MP, Noguchi M, Kishi K, Makuuchi M, Yamasaki S, Hasegawa H, Takayasu K, Moriyama N. Pathology of small hepatocellular carcinoma. A proposal for a new gross classification. *Cancer* 1987; **60**: 810-819

33 **Nakashima O**, Kojiro M. Recurrence of hepatocellular carcinoma: multicentric occurrence or intrahepatic metastasis? A viewpoint in terms of pathology. *J Hepatobiliary Pancreat Surg* 2001; **8**: 404-409

34 **Kojiro M**. 'Nodule-in-nodule' appearance in hepatocellular carcinoma: its significance as a morphologic marker of dedifferentiation. *Intervirology* 2004; **47**: 179-183

35 **Kojiro M**. Diagnostic discrepancy of early hepatocellular carcinoma between Japan and West. *Hepatol Res* 2007; **37** Suppl 2: S121-S124

36 **Kojiro M**, Roskams T. Early hepatocellular carcinoma and dysplastic nodules. *Semin Liver Dis* 2005; **25**: 133-142

37 **Shimada M**, Rikimaru T, Hamatsu T, Yamashita Y, Terashi T, Taguchi K, Tanaka S, Shirabe K, Sugimachi K. The role of macroscopic classification in nodular-type hepatocellular carcinoma. *Am J Surg* 2001; **182**: 177-182

38 **Hui AM**, Takayama T, Sano K, Kubota K, Akahane M, Ohtomo K, Makuuchi M. Predictive value of gross classification of hepatocellular carcinoma on recurrence and survival after hepatectomy. *J Hepatol* 2000; **33**: 975-979

39 **Makuuchi M**, Hasegawa H, Yamazaki S, Bandai Y, Watanabe G, Ito T. Ultrasonic characteristics of the small hepatocellular carcinoma. *Ultrasound Med Biol* 1983; **Suppl 2**: 489-491

40 **Matsui O**. Detection and characterization of small hepatocellular carcinoma. *J Gastroenterol Hepatol* 2004; **19**: S266-S269

41 **Shibata T**, Sakahara H, Kawakami S, Konishi J. Sonographic characteristics of recurrent hepatocellular carcinoma. *Eur Radiol* 1996; **6**: 443-447

42 **Choi BI**, Kim CW, Han MC, Kim CY, Lee HS, Kim ST, Kim YI. Sonographic characteristics of small hepatocellular carcinoma. *Gastrointest Radiol* 1989; **14**: 255-261

43 **Tochio H**, Kudo M. Afferent and efferent vessels of premalignant and overt hepatocellular carcinoma: observation by color Doppler imaging. *Intervirology* 2004; **47**: 144-153

44 **Kudo M**, Tochio H. Intranodular blood supply correlates well with biological malignancy grade determined by tumor growth rate in pathologically proven hepatocellular carci-

noma. *Oncology* 2008; **75** Suppl 1: 55-64
45 **Tanaka S**, Kitamura T, Imaoka S, Sasaki Y, Taniguchi H, Ishiguro S. Hepatocellular carcinoma: sonographic and histologic correlation. *AJR Am J Roentgenol* 1983; **140**: 701-707
46 **Kudo M**. Multistep human hepatocarcinogenesis: correlation of imaging with pathology. *J Gastroenterol* 2009; **44** Suppl 19: 112-118
47 **Ogata R**, Majima Y, Tateishi Y, Kuromatsu R, Shimauchi Y, Torimyra T, Tanaka M, Kumashiro R, Kojiro M, Sata M. Bright loop appearance; a characteristic ultrasonography sign of early hepatocellular carcinoma. *Oncol Rep* 2000; **7**: 1293-1298
48 **Tochio H**, Tomita S, Kudo M, Iwasaki N, Tamura S, Nakamura H, Soga T, Fukunaga T, Okabe Y, Kashida H, Hirasa M, Ibuki Y, Morimoto Y, Orino A. The efferent blood flow of early hepatocellular carcinoma and borderline lesions: Demonstration by color Doppler imaging. *J Med Ultrason* 2002; **29**: 205-209
49 **Zavadsky KE**, Lee YT. Liver metastases from colorectal carcinoma: incidence, resectability, and survival results. *Am Surg* 1994; **60**: 929-933
50 **Roukos DH**. Current advances and changes in treatment strategy may improve survival and quality of life in patients with potentially curable gastric cancer. *Ann Surg Oncol* 1999; **6**: 46-56
51 **Lazaridis G**, Pentheroudakis G, Fountzilas G, Pavlidis N. Liver metastases from cancer of unknown primary (CUPL): a retrospective analysis of presentation, management and prognosis in 49 patients and systematic review of the literature. *Cancer Treat Rev* 2008; **34**: 693-700
52 **Roach H**, Whipp E, Virjee J, Callaway MP. A pictorial review of the varied appearance of atypical liver metastasis from carcinoma of the breast. *Br J Radiol* 2005; **78**: 1098-1103
53 **Robinson PJ**. Imaging liver metastases: current limitations and future prospects. *Br J Radiol* 2000; **73**: 234-241
54 **Marchal GJ**, Pylyser K, Tshibwabwa-Tumba EA, Verbeken EK, Oyen RH, Baert AL, Lauweryns JM. Anechoic halo in solid liver tumors: sonographic, microangiographic, and histologic correlation. *Radiology* 1985; **156**: 479-483
55 **Machi J**, Isomoto H, Kurohiji T, Yamashita Y, Shirouzu K, Kakegawa T, Sigel B, Zaren HA, Sariego J. Accuracy of intraoperative ultrasonography in diagnosing liver metastasis from colorectal cancer: evaluation with postoperative follow-up results. *World J Surg* 1991; **15**: 551-556; discussion 557
56 **Choti MA**, Kaloma F, de Oliveira ML, Nour S, Garrett-Mayer ES, Sheth S, Pawlik TM. Patient variability in intraoperative ultrasonographic characteristics of colorectal liver metastases. *Arch Surg* 2008; **143**: 29-34; discussion 35
57 **Yoshida T**, Matsue H, Okazaki N, Yoshino M. Ultrasonographic differentiation of hepatocellular carcinoma from metastatic liver cancer. *J Clin Ultrasound* 1987; **15**: 431-437
58 **Choi BI**, Kim TK, Han JK, Chung JW, Park JH, Han MC. Power versus conventional color Doppler sonography: comparison in the depiction of vasculature in liver tumors. *Radiology* 1996; **200**: 55-58
59 **Konopke R**, Kersting S, Bergert H, Bloomenthal A, Gastmeier J, Saeger HD, Bunk A. Contrast-enhanced ultrasonography to detect liver metastases : a prospective trial to compare transcutaneous unenhanced and contrast-enhanced ultrasonography in patients undergoing laparotomy. *Int J Colorectal Dis* 2007; **22**: 201-207
60 **Nicolau C**, Vilana R, Catalá V, Bianchi L, Gilabert R, García A, Brú C. Importance of evaluating all vascular phases on contrast-enhanced sonography in the differentiation of benign from malignant focal liver lesions. *AJR Am J Roentgenol* 2006; **186**: 158-167
61 **Furuse J**, Nagase M, Ishii H, Yoshino M. Contrast enhancement patterns of hepatic tumours during the vascular phase using coded harmonic imaging and Levovist to differentiate hepatocellular carcinoma from other focal lesions. *Br J Radiol* 2003; **76**: 385-392
62 **Hatanaka K**, Kudo M, Minami Y, Ueda T, Tatsumi C, Kitai S, Takahashi S, Inoue T, Hagiwara S, Chung H, Ueshima K, Maekawa K. Differential diagnosis of hepatic tumors: value of contrast-enhanced harmonic sonography using the newly developed contrast agent, Sonazoid. *Intervirology* 2008; **51** Suppl 1: 61-69
63 **Hatanaka K**, Kudo M, Minami Y, Maekawa K. Sonazoid-enhanced ultrasonography for diagnosis of hepatic malignancies: comparison with contrast-enhanced CT. *Oncology* 2008; **75** Suppl 1: 42-47
64 **Dietrich CF**, Ignee A, Trojan J, Fellbaum C, Schuessler G. Improved characterisation of histologically proven liver tumours by contrast enhanced ultrasonography during the portal venous and specific late phase of SHU 508A. *Gut* 2004; **53**: 401-405
65 **Albrecht T**, Hoffmann CW, Schmitz SA, Schettler S, Overberg A, Germer CT, Wolf KJ. Phase-inversion sonography during the liver-specific late phase of contrast enhancement: improved detection of liver metastases. *AJR Am J Roentgenol* 2001; **176**: 1191-1198
66 **Nakajima T**, Kondo Y, Miyazaki M, Okui K. A histopathologic study of 102 cases of intrahepatic cholangiocarcinoma: histologic classification and modes of spreading. *Hum Pathol* 1988; **19**: 1228-1234
67 **Clemett AR**. Carcinoma of the major bile ducts. *Radiology* 1965; **84**: 894-903
68 **Khan SA**, Davidson BR, Goldin R, Pereira SP, Rosenberg WM, Taylor-Robinson SD, Thillainayagam AV, Thomas HC, Thursz MR, Wasan H. Guidelines for the diagnosis and treatment of cholangiocarcinoma: consensus document. *Gut* 2002; **51** Suppl 6: VI1-VI9
69 **Yamanaka N**, Okamoto E, Ando T, Oriyama T, Fujimoto J, Furukawa K, Tanaka T, Tanaka W, Nishigami T. Clinicopathologic spectrum of resected extraductal mass-forming intrahepatic cholangiocarcinoma. *Cancer* 1995; **76**: 2449-2456
70 **Colli A**, Cocciolo M, Mumoli N, Cesarini L, Prisco A, Gaffuri I, Martinez E. Peripheral intrahepatic cholangiocarcinoma: ultrasound findings and differential diagnosis from hepatocellular carcinoma. *Eur J Ultrasound* 1998; **7**: 93-99
71 **Sainani NI**, Catalano OA, Holalkere NS, Zhu AX, Hahn PF, Sahani DV. Cholangiocarcinoma: current and novel imaging techniques. *Radiographics* 2008; **28**: 1263-1287
72 **Donato F**, Gelatti U, Tagger A, Favret M, Ribero ML, Callea F, Martelli C, Savio A, Trevisi P, Nardi G. Intrahepatic cholangiocarcinoma and hepatitis C and B virus infection, alcohol intake, and hepatolithiasis: a case-control study in Italy. *Cancer Causes Control* 2001; **12**: 959-964
73 Liver Cancer Study Group of Japan. 1st ed. Tokyo: Kanehara Shuppan, 1997
74 **Yamamoto M**, Takasaki K, Yoshikawa T, Ueno K, Nakano M. Does gross appearance indicate prognosis in intrahepatic cholangiocarcinoma? *J Surg Oncol* 1998; **69**: 162-167
75 **Lim JH**. Cholangiocarcinoma: morphologic classification according to growth pattern and imaging findings. *AJR Am J Roentgenol* 2003; **181**: 819-827
76 **Yoon KH**, Ha HK, Kim CG, Roh BS, Yun KJ, Chae KM, Lim JH, Auh YH. Malignant papillary neoplasms of the intrahepatic bile ducts: CT and histopathologic features. *AJR Am J Roentgenol* 2000; **175**: 1135-1139
77 **Terada T**, Kida T, Nakanuma Y, Noguchi T. Extensive portal tumor thrombi with portal hypertension in an autopsy case of intrahepatic cholangiocarcinoma. *Am J Gastroenterol* 1992; **87**: 1513-1518
78 **Neumaier CE**, Bertolotto M, Perrone R, Martinoli C, Loria F, Silvestri E. Staging of hilar cholangiocarcinoma with ultrasound. *J Clin Ultrasound* 1995; **23**: 173-178
79 **Xu HX**, Lu MD, Liu GJ, Xie XY, Xu ZF, Zheng YL, Liang JY. Imaging of peripheral cholangiocarcinoma with low-mechanical index contrast-enhanced sonography and SonoVue: initial experience. *J Ultrasound Med* 2006; **25**: 23-33

S- Editor Cheng JX **L- Editor** Kerr C **E- Editor** Zheng XM

World Journal of Gastroenterology

Online Submissions: http://www.wjgnet.com/1007-9327office
wjg@wjgnet.com
doi:10.3748/wjg.v16.i33.4187

World J Gastroenterol 2010 September 7; 16(33): 4187-4192
ISSN 1007-9327 (print)

BRIEF ARTICLE

Diagnostic sensitivity of imaging modalities for hepatocellular carcinoma smaller than 2 cm

Keiji Mita, Soo Ryang Kim, Masatoshi Kudo, Susumu Imoto, Taisuke Nakajima, Kenji Ando, Katsumi Fukuda, Toshiyuki Matsuoka, Yoko Maekawa, Yoshitake Hayashi

Keiji Mita, Soo Ryang Kim, Susumu Imoto, Taisuke Nakajima, Kenji Ando, Katsumi Fukuda, Department of Gastroenterology, Kobe Asahi Hospital, Kobe 653-0801, Japan
Masatoshi Kudo, Department of Gastroenterology and Hepatology, Kinki University School of Medicine, Osakasayama 589-8511, Japan
Toshiyuki Matsuoka, Department of Radiology, Osaka City University Medical School, Osaka 558-8585, Japan
Yoko Maekawa, Department of Surgery, Hyogo Cancer Center, Akashi 673-8558, Japan
Yoshitake Hayashi, Center for Infectious Diseases, Kobe University Graduate School of Medicine, Kobe 650-0017, Japan
Author contributions: Mita K, Nakajima T and Ando K designed and performed the majority of imaging examinations; Maekawa Y and Fukuda K were involved in editing the manuscript; Imoto S provided the patient data; Kudo M and Matsuoka T carried out and reviewed the imaging studies; Kim SR and Hayashi Y made the pathological diagnosis of hepatocellular carcinoma; Kim SR wrote the paper.
Correspondence to: Dr. Soo Ryang Kim, Department of Gastroenterology, Kobe Asahi Hospital, 3-5-25 Bououji-cho, Nagata-ku, Kobe 653-0801, Japan. asahi-hp@arion.ocn.ne.jp
Telephone: +81-78-6125151 Fax: +81-78-6125152
Received: March 12, 2010 Revised: May 4, 2010
Accepted: May 11, 2010
Published online: September 7, 2010

Abstract

AIM: To compare the imaging results with histology and to evaluate the diagnostic sensitivity of imaging modalities for hepatocellular carcinoma (HCC) smaller than 2 cm.

METHODS: Nodules smaller than 2 cm (n = 34) revealed by ultrasonography (US) in 29 patients with liver cirrhosis were analyzed. Histological diagnosis of HCC was performed by ultrasonographic guidance: moderately-differentiated HCC (n = 24); well-differentiated HCC (n = 10). The patterns disclosed by the four imaging modalities defined the conclusive diagnosis of HCC: (1) contrast-enhanced computed tomography (CECT), hypervascularity in the arterial phase and washout in the equilibrium phase; (2) Sonazoid contrast-enhanced US (CEUS), hypervascularity in the early vascular phase and defect in the Kupffer phase; (3) gadolinium-ethoxybenzyl-diethylenetriamine pentaacetic acid (Gd-EOB-DTPA)-enhanced magnetic resonance imaging (MRI), hypervascularity in the arterial phase and/or defect in the hepatobiliary phase; and (4) CT arterioportal angiography: hypervascularity by CT during arteriography and/or perfusion defect by CT during arterial portography.

RESULTS: Overall, the sensitivity of diagnosing HCC smaller than 2 cm was 52.9% (18/34) (95% CI: 35.1-70.2) by CECT; 67.6% (23/34) (95% CI: 49.5-82.6) by Sonazoid CEUS; 76.5% (26/34) (95% CI: 58.8-89.3) by Gd-EOB-DTPA MRI; and 88.2% (30/34) (95% CI: 72.5-96.7) by CT arterioportal angiography. The diagnostic sensitivity of detecting moderately-differentiated HCC by CECT, Sonazoid CEUS, Gd-EOB-DTPA MRI and CT arterioportal angiography was 62.5% (15/24) (95% CI: 40.6-81.2), 79.2% (19/24) (95% CI: 57.8-92.9), 75.0% (18/24) (95% CI: 53.3-90.2) and 95.8% (23/24) (95% CI: 78.9-99.9), respectively. A significant difference (P < 0.05) was observed between CECT and CT arterioportal angiography in all nodules. There was no difference between Sonazoid CEUS, Gd-EOB-DTPA MRI, and CT arterioportal angiography. The combined sensitivity of Sonazoid CEUS and Gd-EOB-DTPA MRI was 94.1% (32/34).

CONCLUSION: Changing the main diagnostic modality for HCC smaller than 2 cm from CT arterioportal angiography to Sonazoid CEUS and Gd-EOB-DTPA MRI is recommended.

Key words: Computed tomography arterioportal angiography; Contrast-enhanced computed tomography; Diagnostic sensitivity; Gd-EOB-DTPA-enhanced magnetic

resonance imaging; Hepatocellular carcinoma smaller than 2 cm: Sonazoid contrast-enhanced ultrasonography

Peer reviewers: Søren Rafaelsen, MD, Consultant Radiologist, Associate Professor, Department of Radiology, Vejle Hospital, Vejle, 7100, Denmark; Bernardo Frider, MD, Professor, Department of Hepatology, Hospital General de Agudos Cosme Argerich, Alte Brown 240, Buenos Aires 1155, Argentina

Mita K, Kim SR, Kudo M, Imoto S, Nakajima T, Ando K, Fukuda K, Matsuoka T, Maekawa Y, Hayashi Y. Diagnostic sensitivity of imaging modalities for hepatocellular carcinoma smaller than 2 cm. *World J Gastroenterol* 2010; 16(33): 4187-4192 Available from: URL: http://www.wjgnet.com/1007-9327/full/v16/i33/4187.htm DOI: http://dx.doi.org/10.3748/wjg.v16.i33.4187

INTRODUCTION

The definitive diagnosis of nodular lesions, detected by imaging techniques in the liver with cirrhosis, remains a critical challenge for clinicians. The issue is particularly complicated for small (1-2 cm) nodules, many of which may be preneoplastic with uncertain malignant potential[1], such as macroregenerative nodules, low-grade dysplastic nodules (LGDN) or high-grade dysplastic nodules (HGDN), or more rarely, hemangiomas that are found in up to 42% of explanted livers[2-4].

Recently, clinicians have been able to conduct computed tomography (CT) scanning during angiography, thereby acquiring data on lesions and intranodular blood flow simultaneously[5,6]. To resolve the areas of uncertainty, we have previously reported on the superiority of CT arterioportal angiography [including CT during arteriography (CTA) and CT during arterial portography (CTAP)], concluding that it is superior to contrast-enhanced CT (CECT) and magnetic resonance imaging (MRI) in the diagnosis of hepatocellular carcinoma (HCC) nodules smaller than 2 cm[7].

Moreover, development of the newly introduced diagnostic imaging techniques, Sonazoid contrast-enhanced ultrasonography (CEUS) and gadolinium-ethoxybenzyl-diethylenetriamine pentaacetic acid (Gd-EOB-DTPA)-enhanced MRI have provided higher degrees of detectability for small HCC. In this study, we compared the diagnostic sensitivity of CECT, Sonazoid CEUS, Gd-EOB-DTPA MRI, and CT arterioportal angiography in diagnosing HCC in nodules smaller than 2 cm.

MATERIALS AND METHODS

Patients

From April 2008 to December 2009, we analyzed 34 nodules smaller than 2 cm [8-20 mm; mean ± SD 12.7 ± 3.71 mm; the interquartile range (IQR) 10-15 mm] detected by US in 29 patients (13 men and 16 women; aged 55-84 years; mean ± SD 70.5 ± 7.96 years; IQR 67-76 years) with liver cirrhosis related to hepatitis B virus in 1, hepatitis C virus (HCV) in 24, and alcohol in 4. α-fetoprotein (AFP) measured less than 20 ng/mL in 21 patients and was above 21 ng/mL in 8 (Table 1). In this study, one nodule that was not histologically diagnosed as HCC irrespective of compatibility by imaging studies was excluded, and two nodules were excluded because of inconsistency between readers in the imaging results. The study was approved by the Ethics Committee in Kobe Asahi Hospital.

Table 1 Data and characteristics of 29 patients and 34 nodules

Age (yr), range (mean ± SD)	55-84 (70.5 ± 7.96) IQR 67-76
Sex (M/F)	13/16
Cause	
HBV	1
HCV	24
Alcohol	4
AFP (ng/mL)	
< 20	21
> 21	8
Nodule characteristics (mm), range (mean ± SD)	8-20 (12.7 ± 3.71) IQR 10-15
Histological diagnosis of the 34 nodules	
Moderately-differentiated HCC	24
Well-differentiated HCC	10

IQR: Interquartile range; HBV: Hepatitis B virus; HCV: Hepatitis C virus; AFP: α-fetoprotein; HCC: Hepatocellular carcinoma.

CECT

CECT was conducted with the use of helical CT (Siemens, Germany) with precontrast and postcontrast triple-phase (arterial, portal, venous, and equilibrium phases) scans, after the injection of 120 mL of nonionic contrast medium at 3 mL/s; the scans were carried out in a craniocaudal direction with a 5 mm collimation in the other phases. Acquisition of the arterial and equilibrium phases was automatically started at 30 and 180 s, respectively, after the intravenous injection.

CEUS

Ultrasonography was performed using a SSA-660A (Toshiba Medical Systems, Tochigi, Japan). The vascular findings on phase-inversion harmonic US were shown as tumor vessel flow in the early vascular phase about 15-40 s after injection of Sonazoid (GE HealthCare, Piscataway, NJ, USA). The real-time replenishing images were obtained during the vascular phase (< 2 min after the injection) by release burst imaging. Images of the liver parenchyma were obtained in the postvascular Kupffer phase, at least 10 min after the intravenous injection of Sonazoid. Hepatic malignances were visualized as defects in the postvascular phase. An additional contrast agent was injected to confirm tumor vessel flow in the defect, a technique known as defect reperfusion imaging[8].

Gd-EOB-DTPA MRI

Images by MRI scans (Phillips, Netherlands) were obtained by the 1.0-T superconducting system (Gyroscan 10T-NT, Phillips, Netherlands). Enhanced MRI was used to obtain

Table 2 Imaging patterns for the conclusive diagnosis of hepatocellular carcinoma by the four modalities

Modality	Imaging pattern
Contrast-enhanced CT	Hypervascularity in the arterial phase and washout in the equilibrium phase
Sonazoid contrast-enhanced ultrasonography	Hypervascularity in the early vascular phase and defect in the Kupffer phase
Gd-EOB-DTPA magnetic resonance imaging	Hypervascularity in the arterial phase and/or defect in the hepatobiliary phase
CT arterioportal angiography	Hypervascularity by CTA and/or perfusion defect by CTAP

CT: Computed tomography; CTA: CT during arteriography; CTAP: CT during arterial portography; Gd-EOB-DTPA: Gadolinium-ethoxybenzyl-diethylenetriamine pentaacetic acid.

coronal images by the gradient-echo technique (FFG) at 150/3.5 ms TR/TE, 80° flip angle, and 168 × 256 matrix. In each sequence, the respiration suspension time was 20-30 s. Gd-EOB-DTPA (Primovist; Bayer HealthCare, Osaka, Japan) at a dose of 0.025 mmol/kg body weight was injected intravenously as a rapid bolus at 2 mL/s. Dynamic contrast-enhanced MRI was initiated at 30 s, 70 s, 2-3 min and 20 min after the start of the bolus injection to obtain multiphasic (arterial, portal, late, and hepatobiliary) images.

CT arterioportal angiography (CTA and CTAP)

CTA: At angiography, 45 mL of diluted contrast medium was injected through a catheter at 2 mL/s into the common hepatic artery. The whole liver was then scanned at intervals of 5 to 10 mm.

CTAP: At angiography, 115 mL of diluted contrast medium was injected through a catheter at 2 mL/s into the superior mesenteric artery, according to the scanning time of the entire liver using a power injector during sequential scanning of the liver with incremental changes in the position of the table. Infusion of contrast material was initiated 20 s before CTAP. The whole liver was then scanned at intervals of 5 to 10 mm.

US-guided biopsy

US-guided biopsy was carried out with the use of a 21 gauge Majima needle (Top, Japan). The diagnosis of HCC was made by two operators [a physician (K.S.) and a pathologist (Y.H.)] using the same specimen.

Histological diagnosis

Specimens were routinely processed and stained with hematoxylin and eosin and by the Masson trichromatic method. The diagnosis of HCC was made according to the criteria of the International Working Party[1].

Imaging patterns for the conclusive diagnosis of HCC by the four modalities

The following patterns disclosed by the four imaging modalities were defined as the conclusive diagnosis of HCC. (1) CECT: hypervascularity in the arterial phase and washout in the equilibrium phase; (2) Sonazoid CEUS: hypervascularity in the early vascular phase and defect in the Kupffer phase; (3) Gd-EOB-DTPA MRI: hypervascularity in the arterial phase and/or defect in the hepatobiliary phase; and (4) CT arterioportal angiography: hypervascularity by CTA and/or perfusion defect by CTAP (Table 2).

Imaging studies

To minimize differences in the results between the operators, imaging studies were carried out and reviewed by two operators [a physician (M.K.) and a radiologist (T.M.)] using the same examination protocol.

Statistical analysis

The sensitivity for detecting tumors was indicated by the 95% CI. The 95% CI was estimated by F distribution. The level of significance was set at $P < 0.05$.

RESULTS

The 34 nodules were histologically diagnosed as moderately-differentiated (24 nodules) and well-differentiated (10 nodules) HCC (Table 1). For HCC smaller than 2 cm, the overall diagnostic sensitivity was 52.9% (18/34) (95% CI: 35.1-70.2) by CECT; 67.6% (23/34) (95% CI: 49.5-82.6) by Sonazoid CEUS; 76.5% (26/34) (95% CI: 58.8-89.3) by Gd-EOB-DTPA MRI; and 88.2% (30/34) (95% CI: 72.5-96.7) by CT arterioportal angiography, with a significant difference ($P < 0.05$) between CECT and CT arterioportal angiography. The combined sensitivity of Sonazoid CEUS and Gd-EOB-DTPA MRI was 94.1% (32/34). In diagnosing moderately-differentiated HCC, the diagnostic sensitivity of CECT, Sonazoid CEUS, Gd-EOB-DTPA MRI and CT arterioportal angiography was 62.5% (15/24) (95% CI: 40.6-81.2), 79.2% (19/24) (95% CI: 57.8-92.9), 75.0% (18/24) (95% CI: 53.3-90.2) and 95.8% (23/24) (95% CI: 78.9-99.9), respectively. There was no difference between CECT, Sonazoid CEUS, Gd-EOB-DTPA MRI, and CT arterioportal angiography in moderately differentiated HCC. The sensitivity of well-differentiated HCC was not analyzed because of the paucity of cases (Table 3).

Representative cases

Case No. 1: Detection by Gd-EOB-DTPA MRI and arterioportal angiography: In a 67-year-old woman with HCV-related liver cirrhosis (AFP 9.0 ng/mL; PIVKA II 21 mAU/mL), US revealed a 12 mm hyperechoic nodule in segment eight (Figure 1A). Sonazoid CEUS revealed no hypervascularity in the early vascular phase and no defect in the Kupffer phase. CECT revealed no hypervascularity in the arterial phase and washout in the equilibrium phase.

Table 3 Diagnostic sensitivity of hepatocellular carcinoma by the four modalities

Modality	Diagnostic sensitivity			
	All nodules (n = 34)		Moderately-differentiated HCC (n = 24)	
	n (%)	95% CI	n (%)	95% CI
Contrast-enhanced computed tomography	18 (52.9)	35.1-70.2	15 (62.5)	40.6-81.2
Sonazoid contrast-enhanced ultrasonography	23 (67.6)	49.5-82.6	19 (79.2)	57.8-92.9
Gd-EOB-DTPA magnetic resonance imaging	26 (76.5)	58.8-89.3	18 (75.04)	53.3-90.2
Computed tomography arterioportal angiography	30 (88.2)	72.5-96.7	23 (95.8)	78.9-99.9

Gd-EOB-DTPA: Gadolinium-ethoxybenzyl-diethylenetriamine pentaacetic acid; HCC: Hepatocellular carcinoma.

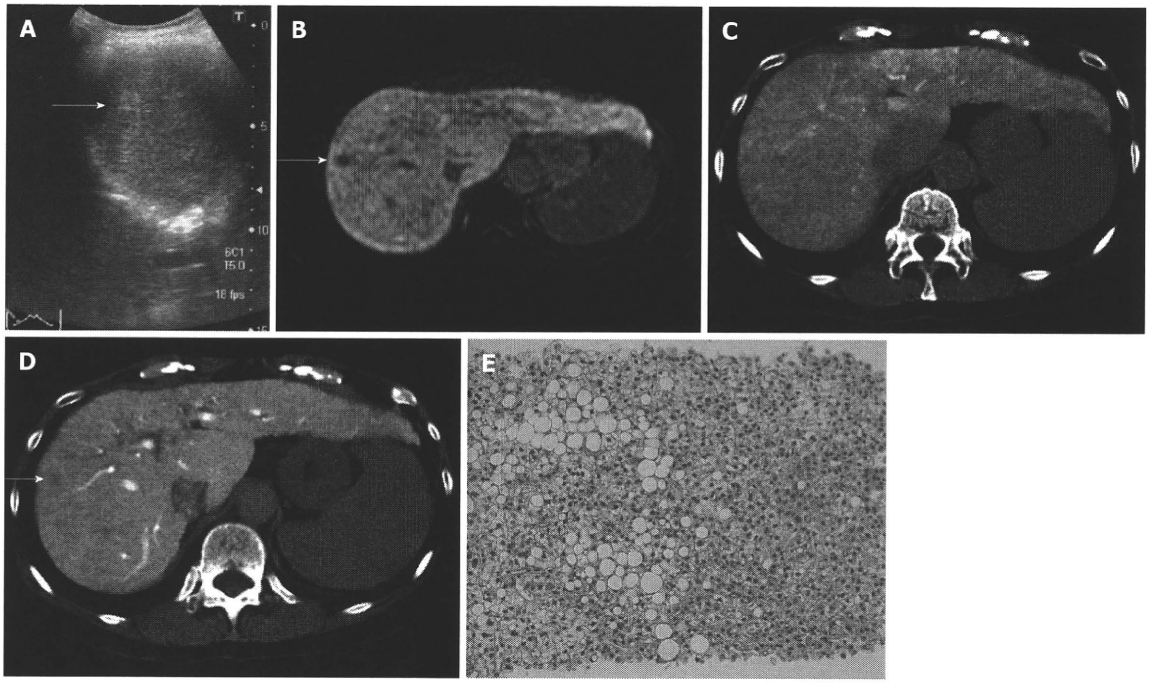

Figure 1 Case No. 1: detection by gadolinium-ethoxybenzyl-diethylenetriamine pentaacetic acid magnetic resonance imaging and computed tomography arterioportal angiography. Imaging and histological findings of the nodule in segment eight. A: Ultrasonography (US) reveals a 12 mm hyperechoic nodule (arrow); B: Gadolinium-ethoxybenzyl-diethylenetriamine pentaacetic acid magnetic resonance imaging reveals a defect (arrow) in the hepatobiliary phase; C, D: Computed tomography during arteriography reveals isodensity (C) and computed tomography during arterial portography (D) reveals a perfusion defect (arrow); E: The nodule is diagnosed as moderately-differentiated hepatocellular carcinoma by US-guided biopsy.

Gd-EOB-DTPA MRI revealed no hypervascularity in the arterial phase, but a defect in the hepatobiliary phase (Figure 1B). CTA revealed isodensity (Figure 1C), and CTAP a perfusion defect (Figure 1D). US-guided biopsy revealed moderately-differentiated HCC (Figure 1E).

Case No. 2: Detection by Gd-EOB-DTPA MRI: In a 74-year-old woman with HCV-related liver cirrhosis (AFP 7.1 ng/mL, PIVKA II 42 mAU/mL), US revealed an 8 mm hyperechoic nodule in segment six (Figure 2A). Sonazoid CEUS revealed no hypervascularity in the early vascular phase and no defect in the Kupffer phase. CECT revealed isodensity in both the arterial phase and the equilibrium phase. MRI revealed isointensity. Gd-EOB-DTPA MRI revealed no hypervascularity in the early phase, but disclosed a defect in the hepatobiliary phase (Figure 2B). CTA revealed no hypervascularity and CTAP no perfusion defect. US-guided biopsy revealed well-differentiated HCC (Figure 2C).

DISCUSSION

Confirmation of arterial hypervascularity by three imaging modalities (triphasic CT, triphasic MRI, and CEUS), even in the absence of a significant (> 400 ng/mL) rise in AFP, is recommended by the European Association for the Study of the Liver (EASL) as diagnostic criteria for HCC nodules larger than 2 cm in patients with cirrhosis[9]. These recommendations for the management of HCC provide a rational approach to the problem but leave some areas of uncertainty, particularly those regarding the interpretation of discordant vascularity, the use of imag-

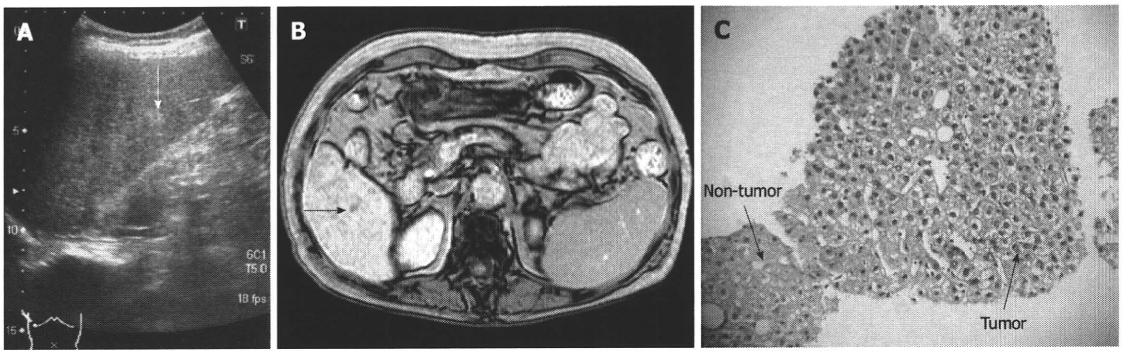

Figure 2 Case No. 2: detection by gadolinium-ethoxybenzyl-diethylenetriamine pentaacetic acid magnetic resonance imaging. Imaging and histological findings of the nodule in segment six. A: Ultrasonography (US) reveals an 8 mm hyperechoic nodule (arrow); B: Gadolinium-ethoxybenzyl-diethylenetriamine pentaacetic acid magnetic resonance imaging reveals a defect (arrow) in the hepatobiliary phase; C: The nodule is diagnosed as well-differentiated hepatocellular carcinoma by US-guided biopsy, showing cellularity more than two-fold that of the non-tumorous area.

ing techniques in nodules smaller than 2 cm, the meaning of truly hypovascular nodules, and the management of those diagnosed with LGDN or HGDN at guided biopsy.

The American Association for the Study of Liver Diseases[2] recommends that the diagnosis of HCC should be made without biopsy when characteristic arterial vascularization and venous washout are observed on three imaging modalities: triphasic CT scan, triphasic MRI and contrast-enhanced harmonic US.

Nevertheless, these recommendations have not been tested and validated except by Bolondi *et al*[10] and Forner *et al*[11]. According to Bolondi *et al*[10], the noninvasive EASL criteria with CEUS and CECT for the diagnosis of HCC are satisfied in only 44% of nodules smaller than 2 cm in cirrhosis. Forner *et al*[11] reported that the diagnostic sensitivity of MRI and CEUS in the diagnosis of HCC (smaller than 2 cm) is 67%.

The main characteristics of Sonazoid, a newly introduced second-generation US contrast agent exclusively approved in Japan in 2007, are that it facilitates real-time blood flow images at low acoustic power and stable Kupffer phase imaging from 10 to 120 min after its injection. In vascular imaging, Sonazoid is considered more effective than Levovist and easy to use; it allows visualization, even with the use of non-high-end equipment and, therefore, reduces dependence on the operator's skills/equipment, all of which may promote the widespread use of CEUS. As stated earlier, Sonazoid CEUS provides very stable postvascular phase images for up to 60-120 min[12], which has resulted in the invention of the breakthrough method, defect reperfusion imaging that is an innovative technology that will greatly change the daily practices of HCC management. In our study, the diagnostic sensitivity of Sonazoid CEUS was 67.6% in all HCC, and 79.2% in moderately-differentiated HCC.

Kudo *et al*[8,13,14] have recently developed defect reperfusion imaging (using the properties of very stable Kupffer phase images and real-time fine blood flow images obtained with Sonazoid) for typical HCC, which is depicted by CT but not by B mode scanning. The method is a breakthrough for accurate localization and treatment guidance[8]: dramatic resolution of many limitations in the diagnosis and treatment of HCC, such as detection of small HCCs[15], evaluation of treatment response[16], and needle insertion guidance; additionally, detection is even more sensitive than with MDCT[15].

A newly introduced contrast agent, Gd-EOB-DTPA, approved in Japan in 2008, is a hepatocyte-specific MRI contrast medium with a different mechanism that utilizes neither dynamic nor Kupffer cell imaging. It is useful in cases which would be difficult to diagnose by techniques such as dynamic MRI or SPIO-MRI. Typical HCC shows high intensity with Gd-EOB-DTPA in the arterial-dominant phase and low intensity in the portal-dominant phase and thereafter. The imaging diagnosis of HCC can be made approximately 10-20 min after the injection of Gd-EOB-DTPA. In our study, the diagnostic sensitivity of Gd-EOB-DTPA MRI was 76.5% in all nodules and 75.0% in moderately-differentiated HCC.

Previously, we had concluded that CT arterioportal angiography was superior to CECT and Gadolinium-enhanced MRI for diagnosing HCC in nodules smaller than 2 cm[7]. In this study, the diagnostic sensitivity of CT arterioportal angiography was 88.2% in all nodules and 95.8% in moderately-differentiated HCC. We observed a significant difference between CECT and CT arterioportal angiography ($P < 0.05$) in all nodules. However, there was no difference between Sonazoid CEUS, Gd-EOB-DTPA MRI, and CT arterioportal angiography. The combined sensitivity of Sonazoid CEUS and Gd-EOB-DTPA MRI in all nodules was 94.1%, due to improvement in the diagnostic capabilities of Sonazoid CEUS and Gd-EOB-DTPA MRI. This improvement in these two imaging modalities with the use of the newly introduced contrast agents provided higher sensitivity for the diagnosis of nodules smaller than 2 cm with Sonazoid CEUS and Gd-EOB-DTPA MRI than with Sonovue CEUS and CECT reported by Bolondi *et al*[10], or with Sonovue CEUS and Gadolinium-enhanced MRI reported by Forner *et al*[11].

These results, considered together with the invasiveness of CT arterioportal angiography, suggest that the principal diagnostic modality for HCC smaller than 2 cm

should be changed from CT arterioportal angiography to Sonazoid CEUS and Gd-EOB-DTPA MRI.

COMMENTS

Background

In spite of the recent advances in imaging techniques, the definitive diagnosis of nodular lesions detected by imaging modalities in the liver with cirrhosis remains a critical challenge for clinicians. The issue is particularly complicated for small (1-2 cm) nodules, many of which may be preneoplastic with uncertain malignant potential. We undertook this study to evaluate the effectiveness of imaging techniques in the diagnosis of hepatocellular carcinoma (HCC) smaller than 2 cm on the basis of histologic findings. Four imaging modalities were compared: contrast-enhanced computed tomography (CECT), Sonazoid contrast-enhanced ultrasonography (CEUS), gadolinium-ethoxybenzyl-diethylenetriamine pentaacetic acid (Gd-EOB-DTPA) magnetic resonance imaging (MRI), and CT arterioportal angiography.

Research frontiers

The authors compared the imaging results with histology and evaluated the diagnostic sensitivity of the 4 imaging modalities.

Innovations and breakthroughs

Previously, the authors had concluded that CT arterioportal angiography was superior to CECT and gadolinium-enhanced MRI for diagnosing HCC in nodules smaller than 2 cm. In this study, the sensitivity of diagnosing 34 HCCs smaller than 2 cm was 52.9% by CECT; 67.6% by Sonazoid CEUS; 76.5% by Gd-EOB-DTPA MRI; and 88.2% by CT arterioportal angiography. A significant difference was observed between CECT and CT arterioportal angiography ($P < 0.05$). There was no difference between Sonazoid CEUS, Gd-EOB-DTPA MRI, and CT arterioportal angiography, and the combined sensitivity of Sonazoid CEUS and Gd-EOB-DTPA MRI was 94.1%, due to improvement in the diagnostic sensitivity of Sonazoid CEUS and Gd-EOB-DTPA MRI. This improvement in these two imaging modalities with the use of the newly introduced contrast agents provided higher sensitivity for the diagnosis of nodules smaller than 2 cm with Sonazoid CEUS and Gd-EOB-DTPA MRI than with Sonovue CEUS and CECT reported by Bolondi *et al*, or with Sonovue CEUS and Gadolinium-enhanced MRI reported by Forner *et al*.

Applications

These results, considered together with the invasiveness of CT arterioportal angiography, suggest that the principal diagnostic modality for HCC smaller than 2 cm should be changed from CT arterioportal angiography to Sonazoid CEUS and Gd-EOB-DTPA MRI.

Peer review

The major strength of the study is that there are many patients with small tumors. The patients have also been applied to new equipment and new contrast substances. It's a very interesting paper.

REFERENCES

1 Terminology of nodular hepatocellular lesions. International Working Party. *Hepatology* 1995; **22**: 983-993

2 **Theise ND**, Schwartz M, Miller C, Thung SN. Macroregenerative nodules and hepatocellular carcinoma in forty-four sequential adult liver explants with cirrhosis. *Hepatology* 1992; **16**: 949-955

3 **Mion F**, Grozel L, Boillot O, Paliard P, Berger F. Adult cirrhotic liver explants: precancerous lesions and undetected small hepatocellular carcinomas. *Gastroenterology* 1996; **111**: 1587-1592

4 **Burrel M**, Llovet JM, Ayuso C, Iglesias C, Sala M, Miquel R, Caralt T, Ayuso JR, Solé M, Sanchez M, Brú C, Bruix J. MRI angiography is superior to helical CT for detection of HCC prior to liver transplantation: an explant correlation. *Hepatology* 2003; **38**: 1034-1042

5 **Hayashi M**, Matsui O, Ueda K, Kawamori Y, Gabata T, Kadoya M. Progression to hypervascular hepatocellular carcinoma: correlation with intranodular blood supply evaluated with CT during intraarterial injection of contrast material. *Radiology* 2002; **225**: 143-149

6 **Tajima T**, Honda H, Taguchi K, Asayama Y, Kuroiwa T, Yoshimitsu K, Irie H, Aibe H, Shimada M, Masuda K. Sequential hemodynamic change in hepatocellular carcinoma and dysplastic nodules: CT angiography and pathologic correlation. *AJR Am J Roentgenol* 2002; **178**: 885-897

7 **Kim SR**, Ando K, Mita K, Fuki S, Ikawa H, Kanbara Y, Imoto S, Matsuoka T, Hayashi Y, Kudo M. Superiority of CT arterioportal angiography to contrast-enhanced CT and MRI in the diagnosis of hepatocellular carcinoma in nodules smaller than 2 cm. *Oncology* 2007; **72** Suppl 1: 58-66

8 **Kudo M**, Hatanaka K, Chung H, Minami Y, Maekawa K. A proposal of novel treatment-assist technique for hepatocellular carcinoma in the sonazoid-enhanced ultrasonography: value of defect re-perfusion imaging (in Japanese). *Kanzo* 2007; **48**: 299-301

9 **Bruix J**, Sherman M, Llovet JM, Beaugrand M, Lencioni R, Burroughs AK, Christensen E, Pagliaro L, Colombo M, Rodés J. Clinical management of hepatocellular carcinoma. Conclusions of the Barcelona-2000 EASL conference. European Association for the Study of the Liver. *J Hepatol* 2001; **35**: 421-430

10 **Bolondi L**, Gaiani S, Celli N, Golfieri R, Grigioni WF, Leoni S, Venturi AM, Piscaglia F. Characterization of small nodules in cirrhosis by assessment of vascularity: the problem of hypovascular hepatocellular carcinoma. *Hepatology* 2005; **42**: 27-34

11 **Forner A**, Vilana R, Ayuso C, Bianchi L, Solé M, Ayuso JR, Boix L, Sala M, Varela M, Llovet JM, Brú C, Bruix J. Diagnosis of hepatic nodules 20 mm or smaller in cirrhosis: Prospective validation of the noninvasive diagnostic criteria for hepatocellular carcinoma. *Hepatology* 2008; **47**: 97-104

12 **Inoue T**, Kudo M, Hatanaka K, Takahashi S, Kitai S, Ueda T, Ishikawa E, Hagiwara S, Minami Y, Chung H, Ueshima K, Maekawa K. Imaging of hepatocellular carcinoma: qualitative and quantitative analysis of postvascular phase contrast-enhanced ultrasonography with sonazoid. Comparison with superparamagnetic iron oxide magnetic resonance images. *Oncology* 2008; **75** Suppl 1: 48-54

13 **Kudo M**, Hatanaka K, Maekawa K. Defect reperfusion imaging, a newly developed novel technology using sonazoid in the treatment of hepatocellular carcinoma. *J Med Ultrasound* 2008; **16**: 169-176

14 **Kudo M**, Hatanaka K, Maekawa K. Sonazoid-enhanced ultrasound in the diagnosis and treatment of hepatic tumors. *J Med Ultrasound* 2008; **16**: 130-139

15 **Hatanaka K**, Kudo M, Minami Y, Maekawa K. Sonazoid-enhanced ultrasonography for diagnosis of hepatic malignancies: comparison with contrast-enhanced CT. *Oncology* 2008; **75** Suppl 1: 42-47

16 **Xia Y**, Kudo M, Minami Y, Hatanaka K, Ueshima K, Chung H, Hagiwara S, Inoue T, Ishikawa E, Kitai S, Takahashi S, Tatsumi C, Ueda T, Hayaishi S, Maekawa K. Response evaluation of transcatheter arterial chemoembolization in hepatocellular carcinomas: the usefulness of sonazoid-enhanced harmonic sonography. *Oncology* 2008; **75** Suppl 1: 99-105

S- Editor Wang JL **L- Editor** Webster JR **E- Editor** Zheng XM

Hepatitis C Virus Core Protein Induces Homotolerance and Cross-Tolerance to Toll-Like Receptor Ligands by Activation of Toll-Like Receptor 2

Hobyung Chung,[1] Tomohiro Watanabe,[2] Masatoshi Kudo,[1] and Tsutomu Chiba[2]

[1]Department of Gastroenterology and Hepatology, Kinki University School of Medicine, Osaka-Sayama, Osaka, and [2]Department of Gastroenterology and Hepatology, Kyoto University Graduate School of Medicine, Kyoto, Japan

Background. Hepatitis C virus (HCV) activates host innate immune responses mediated by retinoic acid inducing gene-I (RIG-I) and Toll-like receptors (TLRs). Although the nonstructural protein 3/4A (NS3/4A) of HCV disrupts interferon responses by inhibiting RIG-I signaling, the effects of TLR activation by HCV-associated proteins on host innate immune responses are poorly understood.

Methods. Proinflammatory cytokine responses to various TLR ligands in human antigen-presenting cells (APCs) were examined either with or without prestimulation by HCV core protein.

Results. TLR2 activation by the HCV core protein leads to a decrease in interleukin 6 (IL-6) production by human APCs after subsequent stimulation with TLR2 (homotolerance) ligands and TLR4 (cross-tolerance) ligands. This hyporesponsiveness induced by preexposure to the HCV core protein was partially mediated by the negative regulation of nuclear factor-κB activation by the induction of IRAK-M. TLR ligand-induced IL-6 production was significantly reduced in peripheral blood monocytes isolated from HCV-infected patients, compared with those of healthy control subjects. Alloantigen presentation by monocytes isolated from HCV-infected patients results in impaired production of interleukin 17 by naive $CD4^+$ T cells in the presence of TLR ligands.

Conclusions. Chronic stimulation of APCs with HCV core protein is associated with hyporesponsiveness in TLR-mediated innate immunity.

Hepatitis C virus (HCV) is a successful pathogen that establishes persistent infection and causes chronic liver disease in the host [1, 2]. The mechanisms by which HCV avoids elimination by the host immune system are poorly understood. One proposed mechanism accounting for the high rate of persistent infection is that HCV infection inhibits the production of type I interferons that constitute the antiviral host defense [3]. HCV RNA is recognized by innate virus-sensing molecules, such as retinoic acid inducing gene-I and Toll-like receptor 3 (TLR3), which then induce rapid interferon responses [4–6]. The HCV nonstructural protein 3/4A protease is reported to blunt the innate antiviral interferon responses mediated by these virus-sensing molecules [5, 7]. However, defective interferon responses are not sufficient to explain the development of the abnormal immunological environments permissive to persistent HCV infection. This notion is supported by the clinical outcome showing that only ~50% of patients with HCV infection are successfully treated with pegylated type I interferon and ribavirin [8].

Several bacterial infections such as sepsis and cellulitis are more common in HCV-infected patients than in those without HCV infection [9–11]. Because TLR-mediated proinflammatory cytokine responses are necessary for host defenses against bacteria [12], it is likely that chronic HCV infection generates an immune environment in which TLR-mediated proinflammatory cytokine production is impaired after exposure to bacterial antigens. With respect to TLR activation by HCV-associated antigens, the core protein activates TLR2 on antigen-presenting cells (APCs) to induce cytokine re-

Received 1 December 2009; accepted 14 April 2010; electronically published 2 August 2010.

Potential conflicts of interest: none reported.

Financial support: This work was supported in part by grants from the Viral Hepatitis Research Foundation of Japan, the Takeda Science Foundation, the Yakult Bioscience Foundation, the Cell Science Research Foundation, and the Uehara Memorial Foundation (to T.W.).

Reprints or correspondence: Dr Tomohiro Watanabe, Department of Gastroenterology and Hepatology, Kyoto University Graduate School of Medicine, 54 Shogoin Kawahara-cho, Sakyo-ku, Kyoto 606-8507, Japan (tmhrwtnb@kuhp.kyoto-u.ac.jp).

The Journal of Infectious Diseases 2010;202(6):853–861

0022-1899/2010/20206-0006$15.00
DOI: 10.1086/655812

sponses through nuclear translocation of nuclear factor-κB (NF-κB) subunits [13, 14]. However, the type of immune response that is finally generated by TLR activation in HCV-infected patients remains largely unknown. If the HCV core protein stimulates TLR2, then this TLR pathway will be constantly activated in peripheral blood APCs in HCV-infected patients. Preactivation of a single TLR pathway results in reduced cytokine responses after restimulation with TLR ligands [15]. Therefore, this study investigated whether the activation of TLR2 by the HCV core protein induces tolerogenic cytokine responses after subsequent stimulation with TLR ligands. We found that core protein–mediated activation of TLR2 in human APCs reduces interleukin 6 (IL-6) production by these cells after restimulation with TLR4 ligands (cross-tolerance), or TLR2 ligands (homotolerance). More importantly, IL-6 production mediated by these TLR ligands is significantly reduced in the peripheral blood monocytes of chronic HCV patients compared with healthy control subjects, resulting in impaired allogeneic interleukin 17 (IL-17) production.

METHODS

Stimulation of cell lines with core protein. Human embryonic kidney 293 (HEK293) cells (ATCC) and isolated clones of HEK293 cells stably expressing the human TLR2 gene (HEK293-TLR2; InvivoGen) or TLR4 and MD2 genes (HEK293-TLR4-MD2; InvivoGen) were stimulated with core protein (2 or 20 μg/mL; Biodesign International), peptidoglycan (10 μg/mL; Fluka), Pam_3CSK4 (10 μg/mL; InvivoGen) or lipopolysaccharide (1 μg/mL; Sigma-Aldrich). The purity of the core protein was >95%. The human monocytic cell line MonoMac 6 (MM6; 1×10^6 cells/mL) [16] was stimulated with core protein (5 μg/mL), peptidoglycan (10 μg/mL), Pam_3CSK4 (10 μg/mL), or lipopolysaccharide (1 μg/mL) in the presence of a neutralizing anti-TLR2 monoclonal antibody (T2.5; 2 or 20 μg/mL; eBioscience) or mouse IgG1 control antibody (eBioscience). Cells were cultured for 24 h, and supernatants were analyzed for production of IL-6 and interleukin 8 (IL-8).

Prestimulation of cells with core protein. Human monocyte-derived dendritic cells (DCs) from healthy control subjects were generated as described elsewhere [17]. DCs or MM6 cells (1×10^6 cells/mL) were incubated with core protein (10 μg/mL) or medium alone for 24 h. The cells were then washed 3 times and restimulated with microbial antigens as described above. Culture supernatants were collected 24 h after restimulation and analyzed for cytokine production.

Flow cytometry. MM6 cells (1×10^6 cells/mL) were incubated with core protein (10 μg/mL) or culture medium alone for 24 h. Cell surface expression of TLR2 and TLR4 was analyzed using a PE-conjugated anti-human TLR2 monoclonal antibody (TL2.1; eBioscience), an anti-TLR4 monoclonal antibody (HTA125; eBioscience) or a PE-conjugated mouse IgG2a control antibody (eBioscience). Apoptotic cell death was assessed using an Annexin V assay as described elsewhere [18]. Cell-surface expression of CD80 and CD86 was analyzed by using a PE-conjugated anti-human CD80 or CD86 monoclonal antibody (eBioscience) as described elsewhere [19].

Enzyme-linked immunosorbent assay. The concentrations of cytokines and chemokines were determined by enzyme-linked immunosorbent assay kits for human IL-6, IL-8, interleukin 10 (IL-10), interleukin 12p40 (IL-12p40), interferon γ (IFN-γ) (BD Bioscience), and IL-17 (eBioscience) as described elsewhere [20].

NF-κB activation assay. Nuclear extracts were prepared from MM6 cells (1×10^6 cells/mL) preincubated with either core protein (10 μg/mL) or medium for 24 h and then stimulated with core protein (5 μg/mL) or lipopolysaccharide (1 μg/mL) for 1 h. The binding of the nuclear extract (30 μg/well) to NF-κB consensus oligonucleotides was measured using a Mercury Transfactor kit (BD Bioscience) as described elsewhere [21].

Immunoblot analysis. Immunoblot analysis was performed as described elsewhere [21]. The blotted membranes were incubated with anti-MyD88 (Active Motif), anti–interferon regulatory factor 3 (IRF3; Santa Cruz Biotechnology), anti–interferon regulatory factor 5 (IRF5; Abcam), anti-IRAK-M (Cell Signalling), or anti-actin (Santa Cruz Biotechnology) antibodies.

Assays with small interfering RNA specific to IRAK-M. MM6 cells (5×10^5 cells/mL) were transfected with either IRAK-M small interfering RNA (siRNA) (Santa Cruz Biotechnology) or control siRNA (25 nmol/L) using the TransIT-TKO transfection reagent (Mirus), followed by stimulation with core protein (10 μg/mL) for 24 h and restimulation with core protein (5 μg/mL) and lipopolysaccharide (1 μg/mL).

Studies using peripheral blood cells from patients. Ethical permission for this study was granted by the review board of Kinki University. Healthy control subjects ($n = 10$) and treatment-naive patients with chronic HCV infection ($n = 10$) were enrolled in this study after informed consent was obtained. Peripheral blood monocytes (1×10^6 cells/mL) isolated from each patient were stimulated with HCV-associated proteins and TLR ligands as described. Monocytes were purified from peripheral blood mononuclear cells (PBMCs) using a monocyte isolation kit (Miltenyi Biotec). Culture supernatants were collected after 24 h and analyzed for cytokine production. In some experiments, monocytes (1×10^6 cells/mL) isolated from HCV patients or healthy control subjects were cocultured for 7 days with naive $CD4^+$ T cells (1×10^6 cells/mL) isolated from PBMCs of healthy control subjects. Culture supernatants were then analyzed for cytokine production. Naive $CD4^+$ T cells were purified using a naive $CD4^+$ T cell isolation kit (Miltenyi Biotec).

This figure is available in its entirety in the online version of the *Journal of Infectious Diseases*.

Figure 1. Hepatitis C virus (HCV) core protein is a specific activator of Toll-like receptor 2 (TLR2).

Statistical analysis. A Student *t* test was used to evaluate statistical significance. Statistical analysis was performed using the StatView software, version 4.5 (Abacus Concepts). A value of $P < .05$ was regarded as statistically significant.

RESULTS

Activation of TLR2 by core protein. Our initial studies determined whether core protein functions as a specific activator of TLR2. Core protein induced IL-8 production only in HEK293-TLR2 cells, which suggests that this protein activates TLR2 (Figure 1*A*). We next used a different approach to confirm this finding in the human monocytic cell line, MM6. Production of IL-6 and IL-8 induced by core protein was reduced by the addition of an anti-TLR2 monoclonal antibody as in the case of stimulation with a conventional TLR2 ligand, peptidoglycan (Figure 1*B*). To further confirm the activation of TLR2 by core protein, we used splenocytes lacking MyD88, a downstream effector molecule of the TLR2 pathway [12]. MyD88-deficient splenocytes failed to produce IL-6 after stimulation with core protein (Figure 1*C*). These data suggest that the core protein is a specific activator of the TLR2-MyD88 signaling pathway.

Induction of cross-tolerance by core protein. Although the ligation of TLRs on APCs induces proinflammatory responses, preexposure to TLR2 or TLR4 ligands has been shown to desensitize APCs to subsequent stimulation by TLRs [22–25]. In the case of the TLR4 signaling pathway, preexposure of APCs to lipopolysaccharide reduces responsiveness not only to lipopolysaccharide (homotolerance) but also to TLR2 ligands (cross-tolerance) [22–25]. It remains controversial whether preactivation of TLR2 leads to cross-tolerance in the TLR4 signaling pathway [22–25]. Identification of core protein as a specific TLR2 activator prompted us to address whether preexposure of APCs to core protein leads to tolerogenic responses not only to TLR2 ligands, but also to TLR4 ligands. For this purpose, MM6 cells were incubated with core protein, followed by stimulation with core protein, peptidoglycan, Pam_3CSK4, or lipopolysaccharide, to measure production of proinflammatory cytokines. Production of IL-6 and IL-8 induced by core protein was markedly reduced in cells prestimulated with core protein compared with cells that were not prestimulated (Figure 2*A*). Interestingly, the production of IL-6 and IL-8 induced by a TLR4 ligand (lipopolysaccharide), as well as TLR2 ligands (peptidoglycan or Pam_3CSK4), was markedly reduced in MM6 cells preincubated with core protein. Preexposure of cells to core protein did not alter the production of IL-12p40 after restimulation with TLR ligands (data not shown). Thus, exposure of MM6 cells to core protein induces homotolerance and cross-tolerance after subsequent stimulation with TLR ligands. We next examined whether this was the case with primary human APCs. Human monocyte-derived DCs from healthy control subjects were activated with core protein and then restimulated with TLR ligands. The production of IL-6 and IL-8 was markedly reduced in DCs after restimulation with TLR2 and TLR4 ligands (Figure 2*B*). Moreover, induction of cross-tolerance by exposure to core protein was impaired by blockade of the TLR2 pathway, because IL-6 production was significantly increased in MM6 cells treated with an anti-TLR2 monoclonal antibody (Figure 2*C*). Taken together, these data strongly suggest that preactivation of TLR2 on human APCs by core protein induces both homotolerance and cross-tolerance after subsequent stimulation with TLR ligands.

Expression of TLRs and activation markers in core protein–tolerant cells. We investigated whether preactivation by core protein alters the expression of costimulatory molecules and TLRs. No significant alteration in the expression of CD80, CD86, TLR2, or TLR4 was seen in MM6 cells by preactivation with core protein (Figure 3*A* and 3*C*). In addition, the expression of CD80 and CD86 was not changed by treatment with core protein after restimulation with core protein or lipopolysaccharide (Figure 3*A*). It is unlikely that the inhibition of TLR responses by core protein prestimulation is due to the induction of apoptotic cell death because stimulation of MM6 cells with core protein did not alter the percentage of Annexin V^+ apoptotic cells (Figure 3*B*).

Molecular mechanisms of cross-tolerance by core protein. NF-κB is a crucial transcription factor for the regulation of IL-6 and IL-8 gene expression. Tolerogenic responses seen after preexposure to Pam_3CSK4 or lipopolysaccharide have been shown to be mediated by a reduction in NF-κB activation [22, 23]. Figure 4*A* shows that after restimulation with either core protein or lipopolysaccharide, the binding of the NF-κB subunits, p65 and p50, from nuclear extracts isolated from MM6 cells preincubated with core protein to consensus sequences is markedly reduced compared with that of cells that had not been preincubated with core protein. In contrast, there was no significant difference in the binding of c-Rel in the nuclear extracts either with, or without, core protein prestimulation. Furthermore, no difference was seen in the binding activity of any of the NF-κB subunits when cells were restimulated with phorbol myristate acetate, which activates NF-κB independent of TLR signaling. Neither the core protein-induced nor lipopolysaccharide-induced binding activity of c-Fos and c-Jun in the nuclear extracts was affected by preincubation with core protein (data not shown). Moreover, p65 nuclear translocation

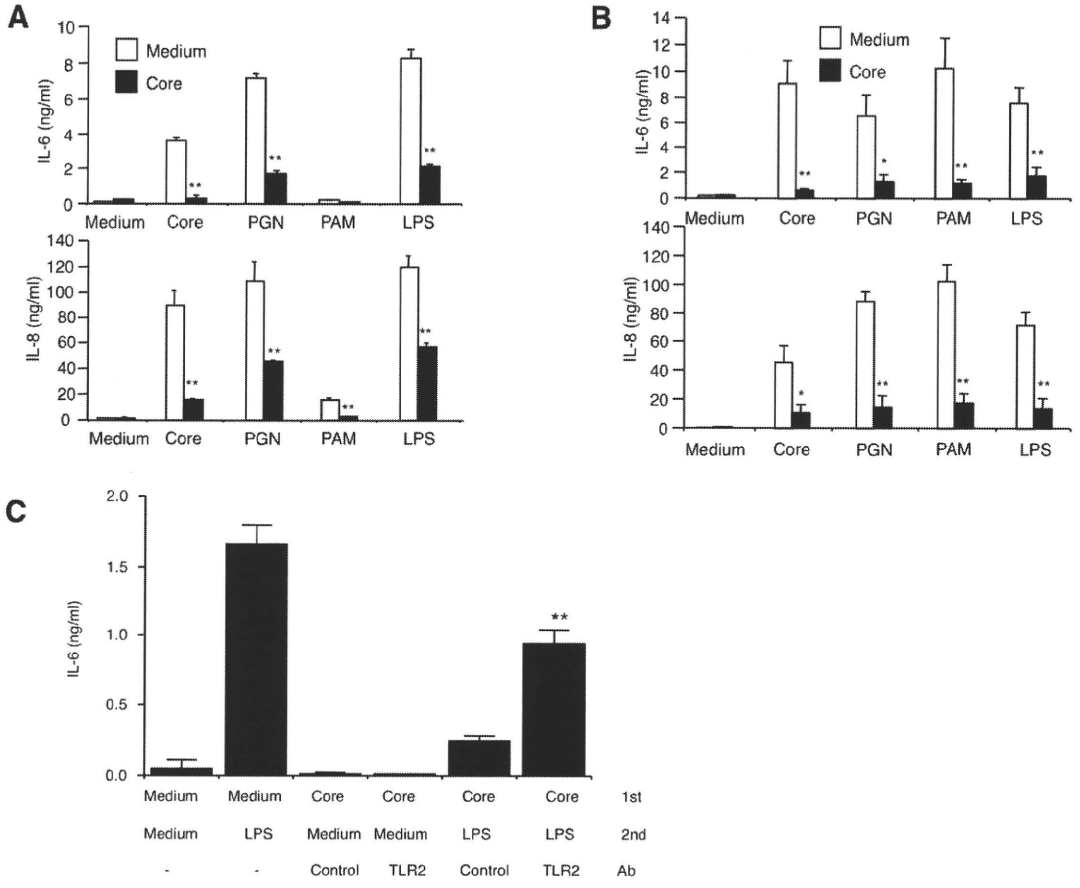

Figure 2. Induction of cross-tolerance to Toll-like receptor (TLR) ligands by hepatitis C virus (HCV) core protein. MM6 cells (1×10^6 cells/mL) (panels *A* and *C*) or human monocyte-derived dendritic cells (DCs) (1×10^6 cells/mL) (panel *B*) were incubated with HCV core protein (10 μg/mL) or culture medium alone for 24 h, washed 3 times, and then stimulated with HCV core protein (5 μg/mL), peptidoglycan (PGN) (10 μg/mL), Pam_3CSK4 (PAM) (10 μg/mL), or lipopolysaccharide (LPS) (1 μg/mL). In some experiments, MM6 cells were treated with anti-TLR2 monoclonal antibody (mAb) (50 μg/mL) or control antibody (Ab) (50 μg/mL) for 12 h before stimulation with core protein. Culture supernatants were collected 24 h later, and production of interleukin 6 (IL-6) and interleukin 8 (IL-8) was measured. *A, C,* Results represent 1 of 3 independent experiments and are shown as mean ± standard deviation. *B,* Results are shown as pooled DCs isolated from 4 healthy control subjects and are expressed as mean ± standard error. $^*P < .05$, $^{**}P < .01$ compared with cells preincubated with medium alone (panels *A* and *B*). $^{**}P < .01$, compared with cells treated with control Ab (panel *C*).

was restored in MM6 cells stimulated with core protein followed by lipopolysaccharide in the presence of an anti-TLR2 monoclonal antibody (Figure 4*B*). These data suggest that core protein prestimulation reduces subsequent activation of NF-κB by TLR ligands.

We performed immunoblot analyses to determine the expression levels of the signaling molecules, or negative regulators, involved in TLR signaling pathways [15] in cells incubated either with, or without, core protein. As shown in Figure 5*A*, there was no difference in the expression of TLR signaling molecules, such as MyD88, IRF3, or IRF5, in cells with or without core protein stimulation. In contrast, core protein clearly enhanced the expression of the negative regulator IRAK-M. A significant reduction in IRAK-M expression was seen in cells treated with an anti-TLR2 monoclonal antibody. We could not detect the expression of other negative regulators such as IRF4 or SOCS-1 by immunoblotting (data not shown). Because IRAK-M is responsible for the induction of endotoxin tolerance [26], we looked at whether IRAK-M expression induced by core protein is involved in the induction of homotolerance and cross-tolerance. We investigated whether gene silencing of IRAK-M expression by siRNA [17] abrogates core protein–mediated inhibitory effects. Figure 5*B* shows that transfection of MM6 cells with IRAK-M siRNA substantially reduced the expression of IRAK-

This figure is available in its entirety in the online version of the *Journal of Infectious Diseases.*

Figure 3. Cell-surface expression of costimulatory molecules and Toll-like receptors (TLRs) in cells stimulated with hepatitis C virus (HCV) core protein.